

This is a repository copy of Thermally-treated asbestos-cement wastes as supplementary precursor for geopolymeric binders: CO2 emission and properties.

White Rose Research Online URL for this paper: <a href="https://eprints.whiterose.ac.uk/id/eprint/232928/">https://eprints.whiterose.ac.uk/id/eprint/232928/</a>

Version: Accepted Version

#### Article:

Santana, H.A. orcid.org/0000-0003-1425-9438, Ruviaro, A.S. orcid.org/0000-0003-0903-7646, Ribeiro, D.V. et al. (3 more authors) (2024) Thermally-treated asbestos-cement wastes as supplementary precursor for geopolymeric binders: CO2 emission and properties. Waste Management, 182. pp. 225-236. ISSN: 0956-053X

https://doi.org/10.1016/j.wasman.2024.04.042

© 2025 The Authors. Except as otherwise noted, this author-accepted version of a journal article published in Waste Management is made available via the University of Sheffield Research Publications and Copyright Policy under the terms of the Creative Commons Attribution 4.0 International License (CC-BY 4.0), which permits unrestricted use, distribution and reproduction in any medium, provided the original work is properly cited. To view a copy of this licence, visit http://creativecommons.org/licenses/by/4.0/

#### Reuse

This article is distributed under the terms of the Creative Commons Attribution (CC BY) licence. This licence allows you to distribute, remix, tweak, and build upon the work, even commercially, as long as you credit the authors for the original work. More information and the full terms of the licence here: https://creativecommons.org/licenses/

#### **Takedown**

If you consider content in White Rose Research Online to be in breach of UK law, please notify us by emailing eprints@whiterose.ac.uk including the URL of the record and the reason for the withdrawal request.



1 2 3	ACTIVATORS ON THE PROPERTIES AND CO <sub>2</sub> EMISSIONS OF METAKAOLIN-BASED GEOPOLYMERS
4	Henrique. A. Santana <sup>1*</sup> , Artur S. Ruviaro <sup>2</sup> , Daniel V. Ribeiro <sup>1</sup> , Marcelo S.
5	Cilla <sup>1</sup> , Brant Walkley <sup>3</sup> , Cleber M. R. Dias <sup>1</sup>
6	(1) Department of Materials Science and Technology (DCTM)/ Federal University of Bahia –
7	Rua Aristides Novis 02, Federação. 40210-630, Salvador/BA, Brazil.
8	(2) Laboratory of Application of Nanotechnology in Civil Construction (LabNANOTEC),
9	Department of Civil Engineering, Federal University of Santa Catarina (UFSC), Brazil
10	(3) Department of Chemical and Biological Engineering, Sir Robert Hadfield Building, The
11	University of Sheffield, Sheffield S1 3JD, United Kingdom.
12	* almeidahen@gmail.com
13	
14	ABSTRACT

This article investigates the effects of thermally treated asbestos-cement waste (ACW<sub>T</sub>) on the properties of metakaolin-based geopolymers prepared with different alkali activators, namely liquid sodium silicate (LSS) and liquid potassium silicate (LKS). Statistical mixture design (SMD) was employed to determine the formulations, which were subjected to a range of tests, including evaluation of rheological parameters (yield stress and apparent viscosity), mineralogical composition using XRD, efflorescence mass, leachate electrical conductivity, compressive strength, and equivalent CO<sub>2</sub> emissions (ECO<sub>2-eq</sub>). The yield stress for formulations produced with sodium silicate ranged from 3.51 Pa to 93.26 Pa, significantly higher than formulations activated with potassium silicate, ranging from 0.03 Pa to 18.80 Pa. However, flash setting was observed in mixtures activated with LKS and containing high percentages of ACW<sub>T</sub>. The mechanical strength and leachate electrical conductivity were found to be significantly affected by the alkali activator content. The ECO<sub>2-eq</sub>, which ranged from approximately 712 to 898 kg CO<sub>2</sub>/m<sup>3</sup> of paste, was higher for formulations activated by LKS but lower for formulations with higher ACW<sub>T</sub> content. Finally, by incorporating ACW<sub>T</sub>, it was possible to optimize the formulations, resulting in high compressive strength and reduced free ions. Overall, this study sheds light on the potential of using ACW<sub>T</sub> in geopolymer-based materials, which can enhance their properties and reduce the negative environmental impact.

**Keywords**: Hazardous waste, environmental analysis, alkali-activated binders, rheology.

32

15

16

17 18

19

20

21

22

23

24

25

26

27

28 29

30

### 1. INTRODUCTION

It is well known that asbestos fibers have the potential to cause cancer [1]. As an environmental and occupational problem, this was one of the reasons that drove the prohibition of the exploitation of this material in over 75 countries [2]. One of the main research priorities is the search for sustainable alternatives for the disposal of asbestos cement waste (ACW) disposed of worldwide.

Based on reverse logistics, researchers have proposed methods to incorporate ACW within cementitious binders, either as a reactive component or a filler material. Thermal treatment inertization [3] stands out as an efficient, safe, and economically competitive process compared to disposal of asbestos in landfills [4]. Through heat treatment, Carneiro et al. [3] established the ideal parameters for inertizing the ACW. They used a 2<sup>k</sup> factorial design in conjunction with a method of simultaneous optimization in order to maximize the belite content (C<sub>2</sub>S) and minimize energy consumption and CO<sub>2</sub> emissions. The ideal values of mass, temperature and calcination time of the material were determined, which can be used as a basis for the design of inertization of other hazardous waste. Asbestos-cement waste after inertization treatment (ACW<sub>T</sub>) has been used in clinker production [5,6], concrete [7], and in the production of alkali-activated binders [8].

In a recent study [9], the production of binary compounds, with the association of ACW<sub>T</sub> with metakaolin, provided matrices of high compressive strength (around 60MPa) and free of efflorescence (unreacted and leached free alkalis). Binary compounds have been previously synthesized using combinations of CaO and Ca(OH)<sub>2</sub> and fly ash [10], fly ash and metakaolin [11], as well as low-calcium fly ash (class F) and high-calcium blast furnace slag [12].

Temuujin et al. [10] evaluated the incorporation of CaO and Ca(OH)<sub>2</sub> in geopolymers based on class F fly ash. The authors observed that the incorporation of calcium improved the mechanical performance of geopolymers through the precipitation of calcium silicate phases aluminate hydrate or calcium silicate hydrate, in addition to favoring the dissolution of fly ash.

Geopolymer systems based on calcium-rich precursors and aluminosilicate precursors can simultaneously form sodium aluminosilicate hydrate (N-A-S-H) and calcium aluminosilicate hydrate (C-A-S-H) gels, with less porous and stronger matrices. However, controlling the properties of a geopolymer binder with a calcium-rich

supplementary precursor, such as ACW<sub>T</sub>, is a challenging task. The inclusion of higher amounts of calcium in geopolymer systems can alter the rheological behavior and reduce the setting time of the mixtures [13], making its consolidation as a cementitious binder unfeasible. Another factor that is still unknown is the influence of the alkali activator (both Na<sup>+</sup> or K<sup>+</sup>-based) in the synthesis of binary composite systems. According to Lu et al. [14], the lower charge density of K<sup>+</sup> provides lower ion-dipole strength and, consequently, lower viscosity of the aluminosilicate precursor-based activating solution.

It was observed that the application of  $ACW_T$  in the production of cementitious binders is possible as long as the behavior of this material is properly known. In this sense, this study provides a comprehensive evaluation of the behavior of geopolymer binders based on metakaolin using  $ACW_T$  as a supplementary precursor and evaluating the influence of the alkali activator (Na or K) on the properties of the matrix. Environmental analysis was also used to determine the effect of alkaline activator and  $ACW_T$  on  $CO_2$  equivalent emissions.

### 2. METHODOLOGY

### 2.1. Materials

Metacaulim HP Ultra from Metacaulim do Brasil Company, and thermally treated asbestos-cement waste (ACW<sub>T</sub>) served as precursors for the experiments. ACW<sub>T</sub> consists of corrugated sheets discarded from buildings after 25 years of use that underwent thermal treatment in a furnace (Linn Elektro Therm GmbH, KK260) at 800 °C for one hour, following the method proposed by Carneiro et al. [3] to eliminate the asbestos fibers. After treatment, the sheets were milled using a ball mill (Quimis, Q298) and passed in a sieve with a mesh opening of 150 μm.

To check the efficiency of thermal treatment to eliminate asbestos in the waste, the ACW and ACW<sub>T</sub> were characterized by X-ray diffraction in a Bruker D2 Phaser diffractometer. Diffraction spectra were obtained for a scanning range  $(2\theta)$  between  $5^{\circ}$  and  $70^{\circ}$ , with a continuous speed of  $0.1^{\circ}$ /s (Fig. 1). The identification of phases was performed using the DiffracEva software and the Crystallography Open Database, and the quantification was carried out using the Rietveld method through the TOPAS software from Bruker. As shown in Fig. 1, chrysotile was not detected in ACW<sub>T</sub>, indicating the complete decomposition of asbestos fibers. The presence of belite (Ca<sub>2</sub>SiO<sub>4</sub>), formed during thermal treatment through the dissociation of CaO from calcite (CaCO<sub>3</sub>) and

association with free SiO<sub>2</sub>, is also observed [15]. It is also noteworthy that belite was formed at a lower temperature than in the production of Portland cement, which generally occurs between 900 and 1250 °C [16], requiring lower energy consumption for forming this phase.

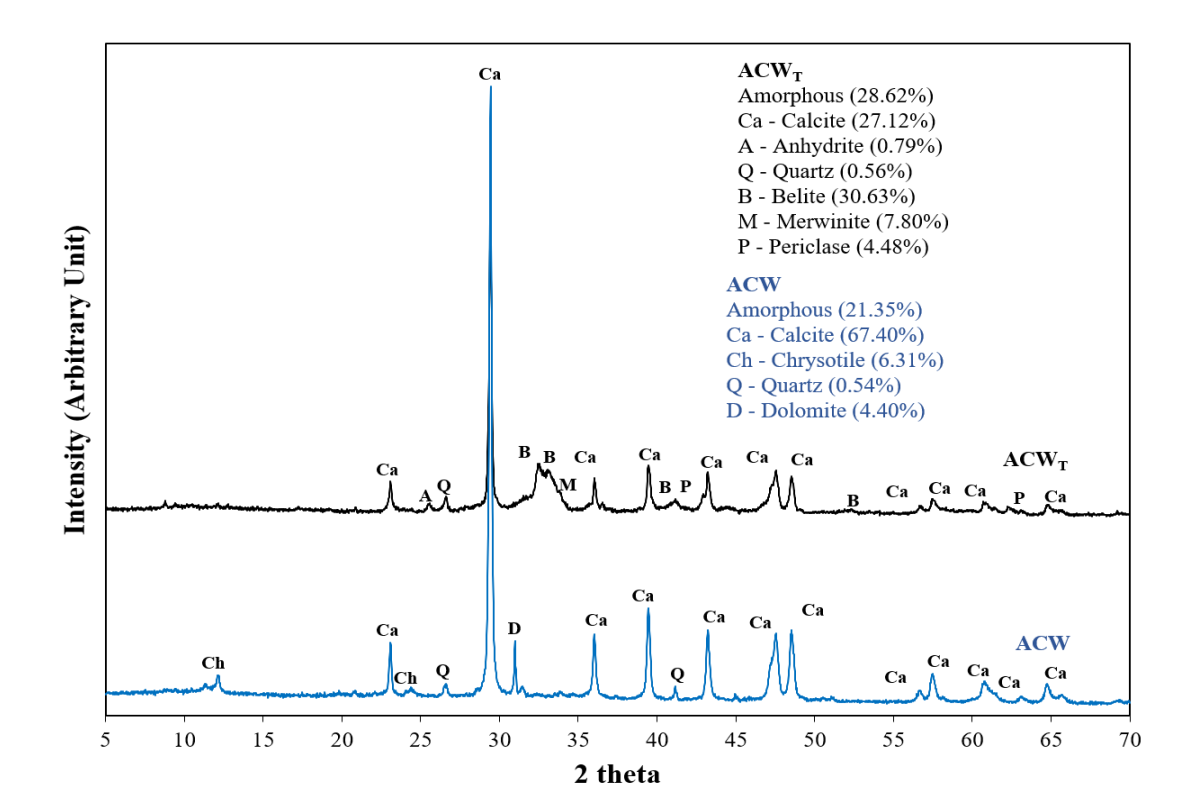


Fig. 1 - X-ray diffraction data with the identification and quantification of the crystalline phases in ACW and ACW<sub>T</sub> samples.

Table 1 shows the skeletal density of metakaolin, silica fume, and  $ACW_T$ , determined by helium gas pycnometer (AccuPyc II 1340 Micromeritics), and their specific surface area determined by the BET method in a Gemini VII Micromeritics Picnometer and the chemical composition obtained by X-ray fluorescence in an S2 Ranger from Bruker XRF Spectrometer.

Table 1 - Chemical composition and physical properties of materials.

Materials	Metakaolin	<b>ACW</b> <sub>T</sub>	Sílica fume
Physical properties			
Skeletal density (g/cm <sup>3</sup> )	2.80	2.95	2.32

BET specific surface area (m²/g)	30.52	6.68	15.15	
Chemical Composition (%)				
$SiO_2$	44.88	18.20	81.75	
$Al_2O_3$	42.86	4.06	1.41	
$Fe_2O_3$	4.82	2.35	4.90	
$K_2O$	0.72	0.34	1.82	
$SO_3$	0.13	1.66	0.51	
MgO	0.67	7.27	1.34	
MnO	0.11	-	0.13	
CaO	-	48.69	0.29	
Others	1.41	1.13	3.46	
Loss on ignition (1000 C)	4.23	16.30	4.40	
				-

It was noted that, although  $ACW_T$  has lower contents of  $Al_2O_3$  and  $SiO_2$  (components that form the N-A-S-H gel) compared to the levels presented by metakaolin, high content of CaO is observed, which can promote the formation of reaction products such as C-S-H and C-A-S-H.

The particle size distribution was determined using a dry laser diffraction particle size analyzer (S3500 Microtrac), and the results are shown in Figure 2. It is observed that  $ACW_T$  presents a particle size distribution close to the metakaolin curve. In addition, the average particle diameter (Dm) of  $ACW_T$  (18.80  $\mu$ m) is close to the value determined for metakaolin (20.29  $\mu$ m).

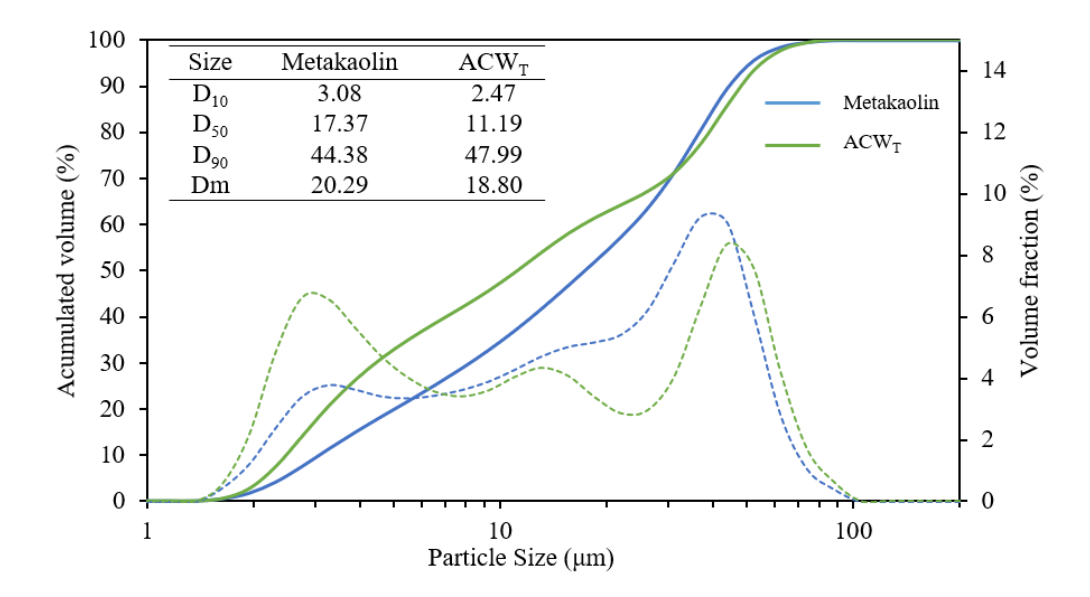


Fig. 2 – Particle size distribution of precursor materials.

Solutions of sodium and potassium silicates were produced in the laboratory to evaluate the influence of the alkali ion type (Na or K) on the chemical reactions of geopolymer matrices produced with aluminosilicates and calcium-rich precursors simultaneously. The solutions were produced with densified silica fume supplied by Companhia de Ferro Ligas da Bahia, sodium hydroxide (NaOH), and potassium hydroxide (KOH), both with 98% purity.

The liquid sodium silicate (LSS) was synthesized with 52% deionized water, 27% SF, and 21% NaOH by mass (molar ratio SiO<sub>2</sub>/Na<sub>2</sub>O equal to 1.33). The liquid potassium silicate (LKS) was produced with 49% deionized water, 27% SF, and 24% KOH by mass (molar ratio SiO<sub>2</sub>/K<sub>2</sub>O equal to 1.16). The silicate solutions were produced with different compositions because NaOH showed higher efficiency in the decomposition reactions of the precursor material in preliminary laboratory tests. The materials were mixed for 60 min using an EDUTEC EEQ-9008 magnetic stirrer. The system was sealed with plastic film to prevent water loss.

### 2.2. Statistical mixture design

The experimental formulations were chosen using the Design-Expert<sup>®</sup> software with the i-Optimal Custom Designs tool and The Best algorithm. In order to establish the mass fractions of the three components of the pastes (metakaolin, ACW<sub>T</sub>, and activating solution), it was necessary to determine both maximum and minimum limits. These limits were based on optimal molar ratios (SiO<sub>2</sub>/Al<sub>2</sub>O<sub>3</sub>, (Na, K)<sub>2</sub>O/Al<sub>2</sub>O<sub>3</sub>, CaO/SiO<sub>2</sub>) that were determined through laboratory tests and literature [17-20]. The ACW<sub>T</sub> was added to the

system, replacing up to 40% (by weight) of the metakaolin and adding CaO to the geopolymer. Table 2 displays the formulations and dosage parameters of the 16 series that were evaluated. All of the formulations were produced with LSS and replicated with LKS.

Table 2 – Weight fractions of the formulations established in the mixture design and their main molar ratios.

E	N	Iass fracti	ions	Silicate/	SiO <sub>2</sub> /	CaO/	LSS	LKS	
Formulations	MK	<b>ACW</b> <sub>T</sub>	Silicate	$(ACW_T+MK)$	Al <sub>2</sub> O <sub>3</sub>	SiO <sub>2</sub>	Na <sub>2</sub> O/Al <sub>2</sub> O <sub>3</sub>	K <sub>2</sub> O/Al <sub>2</sub> O <sub>3</sub>	
F1	0.436	0.040	0.525	1.10	3.16	0.06	0.79	0.64	
F2	0.311	0.089	0.600	1.50	3.89	0.16	1.23	1.01	
F3 and F12	0.251	0.200	0.549	1.22	4.28	0.38	1.33	1.08	
F4, F10 and F11	0.350	0.100	0.550	1.22	3.57	0.17	1.00	0.82	
F5	0.400	0.100	0.500	1.00	3.27	0.16	0.80	0.65	
F6	0.200	0.200	0.600	1.50	5.03	0.39	1.79	1.46	
F7 and F15	0.414	0.000	0.586	1.42	3.31	0.00	0.93	0.76	
F8	0.500	0.000	0.500	1.00	2.93	0.00	0.66	0.54	
F9 and F16	0.325	0.175	0.500	1.00	3.64	0.31	0.96	0.78	
F13	0.360	0.040	0.600	1.50	3.59	0.07	1.08	0.88	
F14	0.254	0.146	0.600	1.50	4.37	0.27	1.47	1.20	
Minimum	0.200	0.000	0.500	1.00	2.93	0.00	0.66	0.54	
Maximum	0.500	0.200	0.600	1.50	5.03	0.39	1.79	1.46	

Eleven formulations were established to estimate the coefficients of the model terms. The remaining series are repetitions of the centroid and strategically selected points to improve the estimates of the model coefficients and the significance of lack of fit. Scheffé's linear polynomial (Eq. 1) is a prediction model that correlates the mixtures' properties with the components' mass fraction.

$$\hat{\mathbf{y}} = \sum_{i=1}^{q} \beta_i \mathbf{X}_i \tag{Eq. 1}$$

where:  $X_i$  is the mass fraction of the  $i_{th}$  components, q is the number of components in the experimental design,  $\hat{y}$  is the value predicted by the model for the property under analysis, and  $\beta_i$  is constant coefficient.  $R^2$ ,  $R_{adj}^2$ ,  $R_{pred}^2$ , the significance of the models and their lack of fit, at a significance level equal to 95% ( $\alpha = 0.05$ ), were used to evaluate the fit quality of the models.

### 2.3. Methods

## 2.3.1 Environmental footprint-related response

For the evaluation of CO<sub>2</sub> equivalent emissions (ECO<sub>2-eq</sub>), the CO<sub>2</sub> equivalent emission of each constituent material of the mixtures was considered (see Table 3).

Table 3 – Specific gravity and equivalent CO<sub>2</sub> emissions of the constituent materials of geopolymer pastes.

Materials	Specific gravity (g/cm³)	ECO <sub>2-eq</sub> (kg of CO <sub>2</sub> /kg of material)	Reference
MK	2.80	0.1960	[21]
$ACW_T$	2.95	0.1665	Calculated
Water	1.00	0.00043	[22]
Sílica fume	2.32	0.0610	Calculated
NaOH	2.13	1.9150	[23]
КОН	2.04	2.2400	[24]

Considering silica fume as a byproduct of iron and steel production, the ECO<sub>2-eq</sub> was disregarded, as recommended by Kong et al. [25], highlighting the environmental importance of incorporating industrial waste and/or byproducts as supplementary cementitious materials. Bajpai et al. [26] also report that silica fume has low ECO<sub>2-eq</sub> related to its beneficiation. Panesar et al. [27] point out that silica fume is a very fine material and does not require additional processing to be used as a supplementary cementitious material, which is why they disregarded the ECO<sub>2-eq</sub>, but emphasize that this is a conservative measure. Therefore, as silica fume is a low-density material, for more precise analysis, the ECO<sub>2-eq</sub> related to transportation was considered. Eq. 2, presented by Ruviaro et al. [28] was used to do so. The transported volume and fuel (diesel) consumption were, respectively, 53 m³ (silo truck) and 2.09 l/km, the same values

presented by the authors. The emission factor of diesel is  $2.614 \text{ kg CO}_{2\text{-eq}}/l$ , as reported by Pervez et al. [29]. The average transport distance suggested in other works was 150 km [28]. The average transport distance considered was 150 km. The calculated unit mass of silica fume is 338 kg/m³. The resulting value was  $0.0610 \text{ kg CO}_{2\text{-eq}}/kg$  of silica fume.

$$E_t = \frac{dm * C}{V * u} * EF$$
 (Eq. 2)

where  $E_t$  is the  $CO_{2-eq}$  emissions per kg of transported material (kg. $CO_{2-eq}$ /kg); dm is the average transport distance (km); C is the vehicle fuel consumption (km/l); V: transport capacity (m³);  $\mu$ : unit mass of transported material (kg/m³); EF: vehicle fuel emission factor (kg  $CO_{2-eq}$ /l).

For the calculation of ECO<sub>2-eq</sub> related to ACW<sub>T</sub>, the processes involved in the beneficiation were considered: calcination, milling, and sieving. Calcination was performed for the decomposition of chrysotile, as reported by Kusiorowski et al. [30]. The milling and sieving processes were carried out after the heat treatment to avoid fiber fragmentation since the size of the fibers (diameter and length) is associated with diseases, as presented in Lippmann [31]. Therefore, the equipment used and the amount of material per production cycle were considered (Table 4).

Table 4 – Beneficiation processes involved in the production of ACW<sub>T</sub>.

Step (equipment)	Potency (P), Watts	Time (T), Minutes	Yield per cycle (η), kg
Calcination (Linn Elektro Therm GmbH, KK260)	1400	110	50
Milling (Quimis, Q298)	150	120	4
Sieving (Solotest, G)	250	20	4

Although the thermal treatment proposed in the literature was designed for calcining a mass of asbestos equal to 5 kg [3], the investigation of ECO<sub>2-eq</sub> was considered using 50% of the furnace capacity, that is, 50 kg per cycle, to approximate the industrial production conditions. The calculation was performed according to Eq. 3, considering the processes shown in Table 4, considering that for every 1 kWh, 0.135 kg of CO<sub>2</sub> is emitted, considering the Brazilian energy matrix [32].

$$CO_{2-eq} = \left[\sum_{i} \frac{P_i \times T_i}{\eta_i}\right] \times \frac{0.135}{60000}$$
 (Eq. 3)

where, CO<sub>2-eq</sub> is the Equivalent CO<sub>2</sub> emissions, in kg CO<sub>2</sub>/kg of ACW;  $P_i$  is the power of equipment i, in W;  $T_i$  is the time per cycle of use of equipment i, in minutes;  $\eta_i$  is the yield per cycle in kg.

For calcination, the heating ramp of the furnace was considered for a heating rate of 10 °C/min until reaching a temperature of 800°C, which has been previously adopted by other authors [33]. During the plateau, the equipment turns on at certain time intervals only to maintain the temperature, so 30 minutes was considered during the 60-minute plateau. It should be noted that these three processes were carried out on a laboratory scale, which, when employed on a larger scale, will certainly be lower than those presented. The total equivalent emissions for ACW<sub>T</sub>, calculated according to Eq.03, are 0.0199 kg CO<sub>2</sub>/kg ACW<sub>T</sub>.

Furthermore, the calcination of ACW converts calcium carbonate present in the waste to calcium oxide ( $CaCO_3 \rightarrow CaO + CO_2$ ), increasing the  $CO_2$  quantities in the equivalent emissions of ACW<sub>T</sub>. To quantify  $CaCO_3$ , the thermogravimetric analysis (Fig. 3) was performed and based on Eq. 4, considering the decomposition of  $CaCO_3$  between 600 - 800 °C, as presented by Scrivener et al. [34]. After determining the mass of calcium carbonate, by stoichiometry, the mass of  $CO_2$  was determined. The calculated percentages of  $CaCO_3$  and  $CO_2$  were 33.34% and 14.66% of the total sample mass, respectively. Therefore, the total equivalent  $CO_2$  emissions are 0.1665 kg  $CO_2$ /kg of  $ACW_T$ .

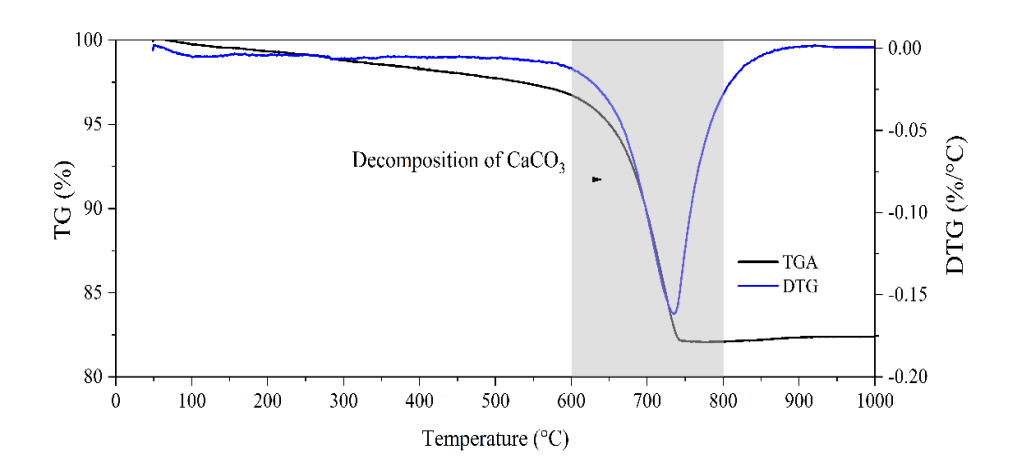


Fig. 3 – Thermogravimetric analysis of ACW.

$$CaCO_3 = WL_{CaCO_3} \times \frac{m_{CaCO_3}}{m_{CO_2}}$$
(Eq. 4)

where:  $CaCO_3$  - Percentage of calcium carbonate (%);  $WL_{CaCO_3}$  - Loss of mass of calcium carbonate;  $m_{CaCO_3}$  - Molar mass of calcium carbonate (100 g/mol);  $m_{CO_2}$  - Molar mass of carbon dioxide (44 g/mol).

For the calculation of the total equivalent CO<sub>2</sub> emissions by composition, the material consumption per m<sup>3</sup> of paste was used, determined based on the mass fractions of the formulations (Table 2) and preliminary tests carried out in the laboratory. Finally, the ECO<sub>2-eq</sub> intensity was calculated, which relates the ECO<sub>2-eq</sub> to the compressive strength of the material, and the results are expressed in (kg CO<sub>2-eq</sub>/m<sup>3</sup>).MPa<sup>-1</sup>.

### 2.3.2. Fresh state responses

The geopolymer pastes were produced in a 5 L planetary mixer. The metakaolin and ACW<sub>T</sub> were mixed for 30 s, followed by the addition of the activator solution for 30 s and mixed for another 30 s. The mixer was turned off for 30 s to scrape the sides and to mix the paddle, and then mixed for another 30 s. The entire process was carried out at a low speed  $(62.5 \pm 5 \text{ rpm})$ .

The rheological properties of the fresh formulations were evaluated using rotational rheometry in a Haake MARS III rheometer (Thermo Fisher Scientific) equipped with cylindrical geometry (diameter of 23.86 mm and height of 34.5 mm) and a 5-mm gap (see Fig. 4a). The measurements were conducted at 23 °C using approximately 7.5 mL of paste samples (see Fig. 4b).

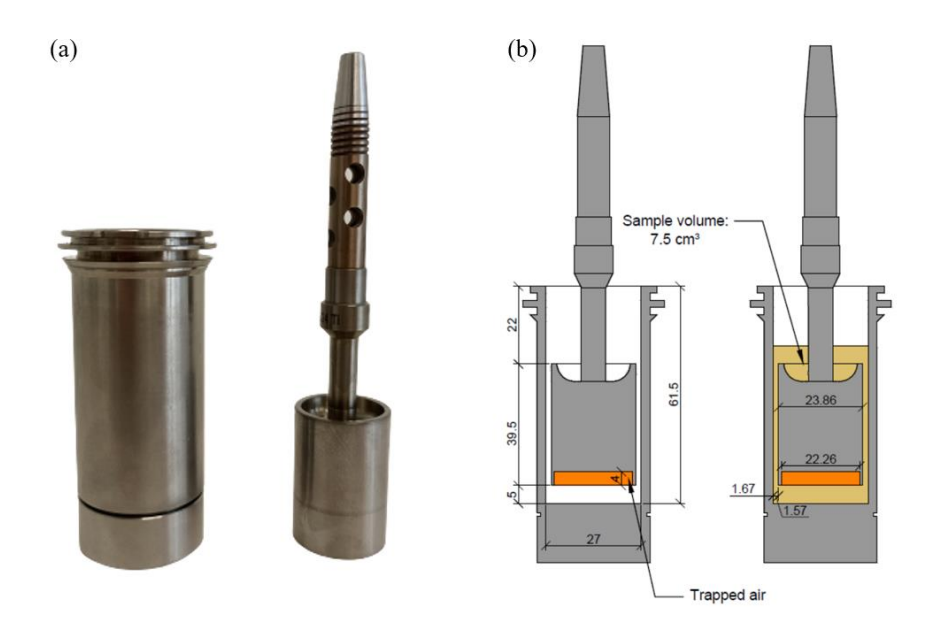


Fig. 4 – Cup and geometry used (a) and test specifications (b).

Figure 5 shows the setup used to obtain the flow curves. Briefly, the flow curves (ascending and descending) were obtained as follows: (i) applying a pre-shear rate of  $100.0~\rm s^{-1}$  for  $60~\rm s$ , (ii) a rest period of  $60~\rm s$ , (iii) the upward flow curve was obtained by increasing the shear rate from  $0.1~\rm s^{-1}$  to  $10.0~\rm s^{-1}$  in four logarithmically distributed steps (Fig. b), and from  $10.0~\rm s^{-1}$  to  $100.0~\rm s^{-1}$  in six linearly distributed steps. The downward flow curve was determined by decreasing the shear rate from  $100.0~\rm s^{-1}$  to  $10.0~\rm s^{-1}$  linearly and from  $10.0~\rm s^{-1}$  to  $0.01~\rm s^{-1}$  logarithmically (Fig. c) in the same steps of the ascending curve. At each step, the shear rate was maintained for  $20~\rm s$ , and only the last  $3~\rm s$  were recorded to ensure a more stable measurement. For greater accuracy in determining yield strength, as suggested by Vance et al. [35], a greater number of readings were performed in the initial and final stretches of the curves with low shear rates (Fig. b and Fig. c).

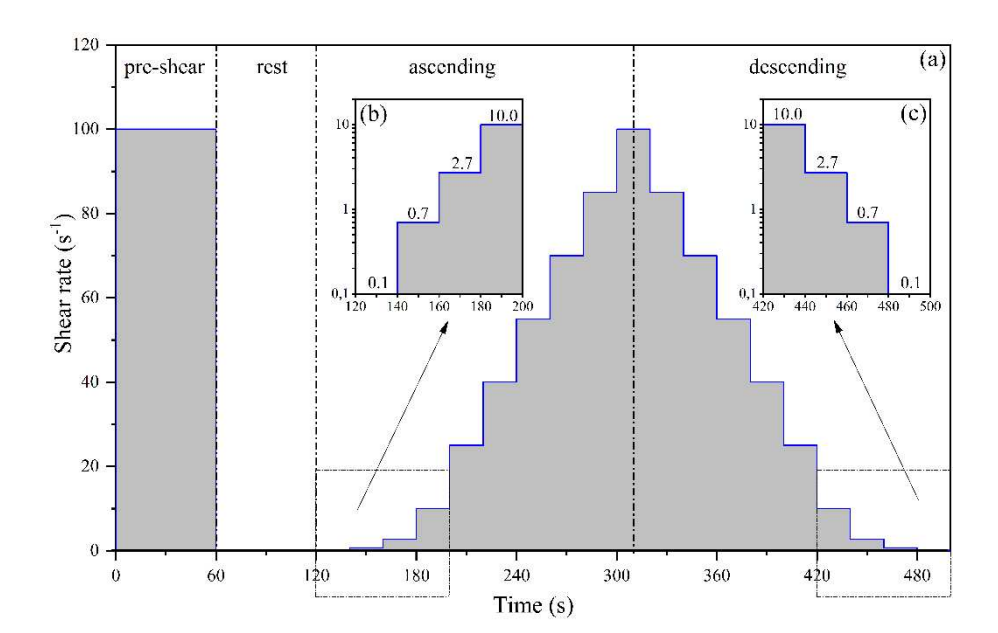


Fig. 5 – Rheological test routine of the pastes (a) and details of the beginning (b) and end (c) of the shear ramps.

The Herschel-Bulkley model (Eq. 5) was used to describe the rheological behavior, and the equivalent viscosity (Eq. 6) was calculated using De Larrard's equation [37].

$$\tau = \tau_0 + K.\dot{\mathbf{y}}^n \tag{Eq. 5}$$

$$\mu_{eq} = \frac{3K}{n+2} \cdot (\dot{y}_{max})^{n-1}$$
 (Eq. 6)

where  $\tau$  is the shear stress (Pa),  $\tau_0$  is the dynamic yield stress (Pa),  $\dot{\gamma}$  is the shear rate (s<sup>-1</sup>), K and n are, respectively, the consistency and the pseudoplastic parameters of the H-B model,  $\mu_{eq}$  is the equivalent viscosity (Pa.s), and  $\dot{\gamma}_{max}$  is the maximum shear rate

292 applied.

### 2.3.3. Hardened state responses

For analysis in a hardened state, the pastes were demolded after 24 hours, and the specimens were cured in an environment with a temperature of  $(25 \pm 2)$  °C and a relative humidity of  $(65 \pm 5)$  % for 28 days.

For the identification of the mineralogical phases, the pastes were analyzed by XRD using a Bruker D2 Phaser Diffractometer. Before analysis, the paste samples were dried in an oven at X  $^{\circ}$ C and then milled using agate mortar and pestle. Samples that passed through a 75- $\mu$ m sieve were utilized for analysis. The diffraction spectra were obtained by scanning a range of (2 $\theta$ ) between 5 $^{\circ}$  and 70 $^{\circ}$  at a continuous speed of 0.1 $^{\circ}$ /s. The phase identification was performed utilizing the DiffracEva software and the Crystallography Open Database.

To determine the compressive strength of the geopolymer pastes, three cubic specimens with 40 mm edge lengths were molded for each formulation. The compressive strength ( $C_S$ ) was determined after 28 days of curing. The test was conducted on a servohydraulic press with a capacity of 1200 kN, applying a loading rate of 500 N/s to the specimens.

The methodology utilized to estimate the content of unreacted ions (Na<sup>+</sup> and K<sup>+</sup>) in the cured pastes was proposed and described by Santana et al. [9] and Longhi et al. [36]. Four cubic specimens per formulation with a 25 mm edge were placed in a Petri dish. They were then covered with a 1 mm layer of water and exposed to an environment with a temperature of  $(24 \pm 2)$  °C and relative humidity of  $(65 \pm 5)$  % for 20 days. The specimens were subjected to daily water replacement to maintain optimal conditions (Fig. 6a). Due to the humidity gradient of the geopolymers pastes, free ions were transported to the surface of the specimens, where they reacted with CO<sub>2</sub>, resulting in efflorescence.

After 20 days of exposure, the pastes were dried in a kiln at  $(40 \pm 2)$  °C for 24 h, weighed on a balance with a precision of 0.001 g (Mi), and placed into an Erlenmeyer flask filled with deionized distilled water up to a volume of 150 ml (Fig. 6b). Following the release of unreacted ions (24 hours of immersion), the electrical conductivity ( $\sigma$ , Ms/cm) of the solution inside the Erlenmeyer flask was measured. The specimens were dried again at  $(40 \pm 2)$  °C, weighed, and their dry mass, free of efflorescent material (Ms), was determined. The mass of the effloresced material (Me) was calculated by subtracting Ms from Mi (Me = Mi - Ms).

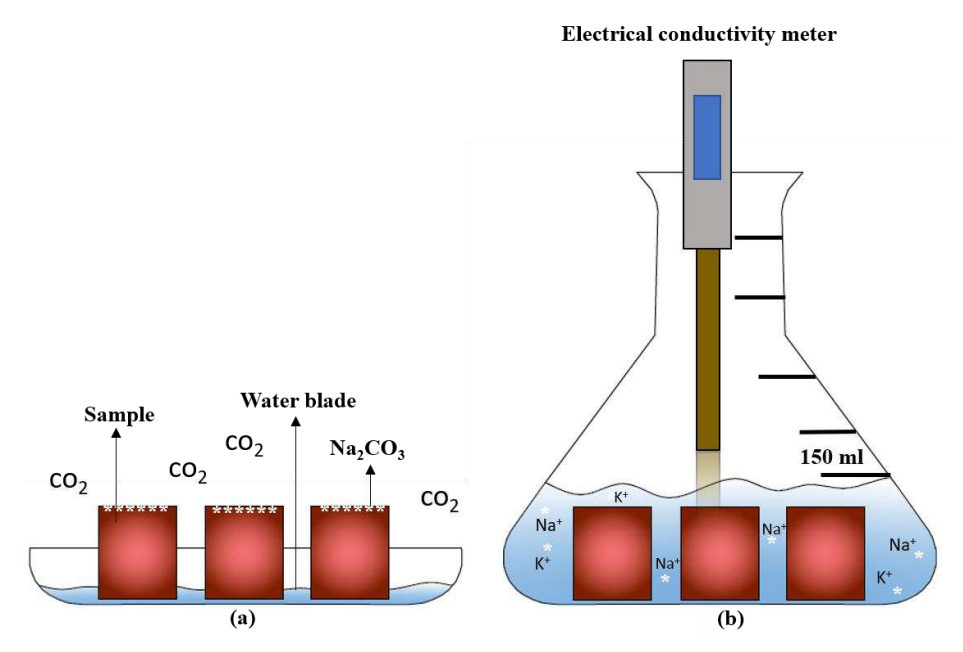


Fig. 6 – Samples (a) submitted to the accelerated efflorescence test and (b) immersed in distilled and deionized water for measurement of conductivity of the solution.

# 3. RESULTS AND DISCUSSIONS

Table 5 presents the greenhouse gas equivalence in carbon dioxide [ECO<sub>2-eq</sub>(kg CO<sub>2</sub>/kg paste)], yield stress values [ $\tau_0$  (Pa)], equivalent viscosity values [ $\mu_{eq}$  (Pa.s)], compressive strength values [ $C_S$  (MPa)], efflorescence mass values [ $E_f$  (g)], and the leachate electrical conductivity values [ $\sigma$  (mS/cm)] for pastes produced with sodium silicate (LSS) and potassium silicate (LKS). As a result of the wide variation of the mass fraction of the mixture components, each property of the formulations varied widely. As an example, the compressive strength varied from 33.2 to 61.3 MPa for LSS and from 30.6 to 62.6 MPa for LKS.

Tabela 5 – Propriedades determinadas para as pastas produzidas com NSS e KSS

	M	ass fractio	ons			Prop	erties (LSS	5)				Properties	(LKS)		
Formulations	MK	<b>ACW</b> <sub>T</sub>	SOL	ECO <sub>2-eq</sub> (kg/kg)	$ au_0$ (Pa)	μ <sub>eq</sub> (Pa.s)	Cs (MPa)	Ef (g)	σ (mS/cm)	ECO <sub>2-eq</sub> (kg/kg)	$ au_0$ (Pa)	μ <sub>eq</sub> (Pa.s)	Cs (MPa)	Ef (g)	σ (mS/cm)
F1	0.436	0.040	0.525	728.26	35.03	5.36	56.05	4.06	13.41	854.28	1.42	1.61	61.72	2.90	12.32
<b>F2</b>	0.311	0.089	0.600	751.40	5.90	1.81	38.70	9.50	27.00	895.46	0.32	0.70	33.97	6.15	27.60
<b>F3</b>	0.251	0.200	0.549	727.29	8.61	3.10	36.89	8.23	32.40	859.04	1.40	1.69	42.75	5.06	21.90
<b>F4</b>	0.350	0.100	0.550	733.45	16.07	3.67	50.39	7.01	21.30	865.52	1.69	1.66	44.58	4.52	19.75
<b>F</b> 5	0.400	0.100	0.500	716.15	41.13	7.38	61.16	3.57	10.20	836.20	1.13	1.14	59.17	1.85	8.99
<b>F6</b>	0.200	0.200	0.600	745.00	3.51	1.49	33.23	10.64	41.10	889.07	1.04	1.04	30.58	7.32	33.50
<b>F7</b>	0.414	0.000	0.586	751.73	14.43	2.82	45.57	5.13	16.70	892.47	0.44	0.53	43.23	3.20	21.50
F8	0.500	0.000	0.500	721.91	93.26	10.47	61.26	3.12	7.62	841.96	4.43	2.38	62.60	2.79	6.42
F9	0.325	0.175	0.500	711.83	30.56	7.85	50.41	3.90	21.40	831.88	2.02	2.58	61.08	2.29	12.20
F10	0.350	0.100	0.550	733.45	16.19	3.55	54.76	6.86	21.40	865.52	1.61	1.63	44.69	4.73	19.22
F11	0.350	0.100	0.550	733.45	15.98	3.69	53.09	6.36	24.80	865.52	1.62	1.69	40.68	4.57	20.01
F12	0.251	0.200	0.549	727.29	8.55	3.08	38.29	8.07	31.90	859.04	1.43	1.50	40.57	5.14	22.50
F13	0.360	0.040	0.600	754.20	8.21	2.23	41.00	7.06	25.20	898.27	0.26	0.48	41.44	4.76	25.40
F14	0.254	0.146	0.600	748.12	4.19	1.72	37.80	8.16	31.70	892.19	1.77	1.60	33.99	5.37	28.70
F15	0.414	0.000	0.586	751.73	14.33	2.91	49.59	4.55	16.51	892.47	0.42	0.55	44.67	4.13	21.42
F16	0.325	0.175	0.500	711.83	28.98	7.81	54.02	4.96	21.70	831.88	2.10	2.63	54.31	3.05	11.13
Minimum	0.200	0.000	0.500	711.83	3.51	1.49	33.23	3.12	7.62	831.88	0.03	0.05	30.58	1.85	6.42
Maximum	0.500	0.200	0.600	754.20	93.26	10.47	61.26	10.64	41.10	898.27	18.80	2.35	62.60	7.32	33.50

## 3.1 CO<sub>2</sub> equivalent emissions

Fig. 7 and Fig. 8 present the results of CO<sub>2</sub> equivalent emissions by LSS- and LKS-activated pastes, respectively. Due to their high environmental burden, activators are responsible for the higher portions of ECO<sub>2-eq</sub>, ranging from 59-69% for NaOH and from 65-74% for KOH, being even more significant for KOH, which presents 14.51% higher ECO<sub>2-eq</sub> compared to NaOH. Turner and Collins [38] showed that the NaOH-based activating solution accounted for ~59% of the total ECO<sub>2-eq</sub> of a geopolymer mixture. Among the metakaolin-based geopolymer mixtures evaluated by Villaquirán-Caicedo and de Gutiérrez [24], the portion of ECO<sub>2-eq</sub> related to KOH ranged from 46-88% of total emissions.

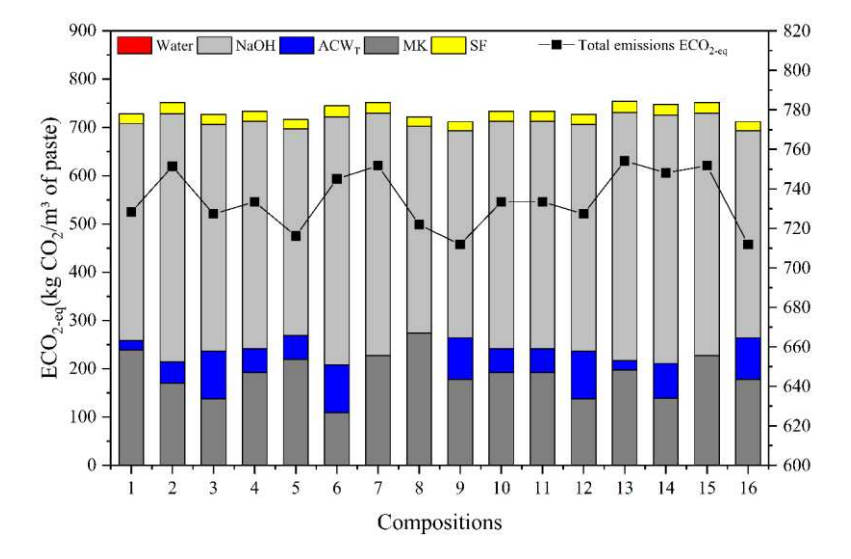


Fig. 3 – Equivalent emissions for LSS activated pastes.

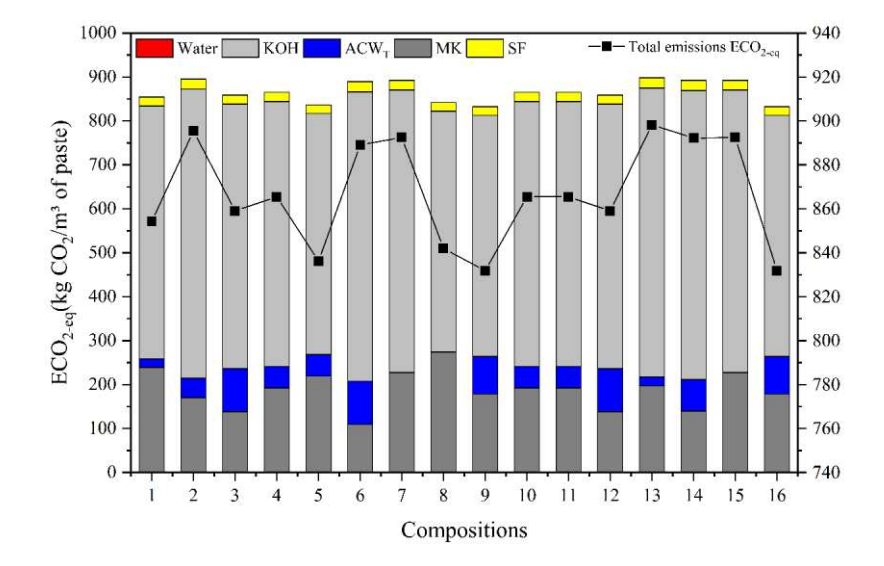


Fig. 8 – Equivalent emissions for LKS activated pastes.

The values presented in this research are high because the calculations are performed for pastes. When geopolymer pastes are used to produce concrete, the values will be lower, considering that approximately 70% of the concrete volume is composed of aggregates [39]. Aggregates have low ECO<sub>2-eq</sub> related to the extraction and processing process, reducing the total ECO<sub>2-eq</sub> of the produced composites. The emissions associated with water were negligible (0.01-0.02%). On the other hand, silica fume contributed to 2-3% of the total ECO<sub>2-eq</sub>, owing to its classification as an industrial residue waste that requires minimal processing to be used.

When considering the precursor materials (MK and ACW<sub>T</sub>), the percentage of ECO<sub>2-eq</sub> related to MK ranged from 15-38% for LSS-activated pastes and 12-33% for LKS-activated pastes. For ACW<sub>T</sub>, the values ranged from 0-14% and 0-11% for LSS-and LKS-activated pastes, respectively. Notably, since these materials are present in larger quantities in the geopolymer binder, the ECO<sub>2-eq</sub> values are lower when compared to those of the activators.

In Fig. 9, a comparison is presented of the  $ECO_{2\text{-eq}}$  if the mixtures were made with 100% MK. Modest reductions are observed, not exceeding 5% of the total  $ECO_{2\text{-eq}}$  related to precursors. Even though  $ACW_T$  has  $ECO_{2\text{-eq}} \sim 15\%$  lower than MK, as the substitution percentage is low, the reductions end up not being significant. However, the incorporation of  $ACW_T$  is extremely important as it provides adequate disposal for material from inert waste.



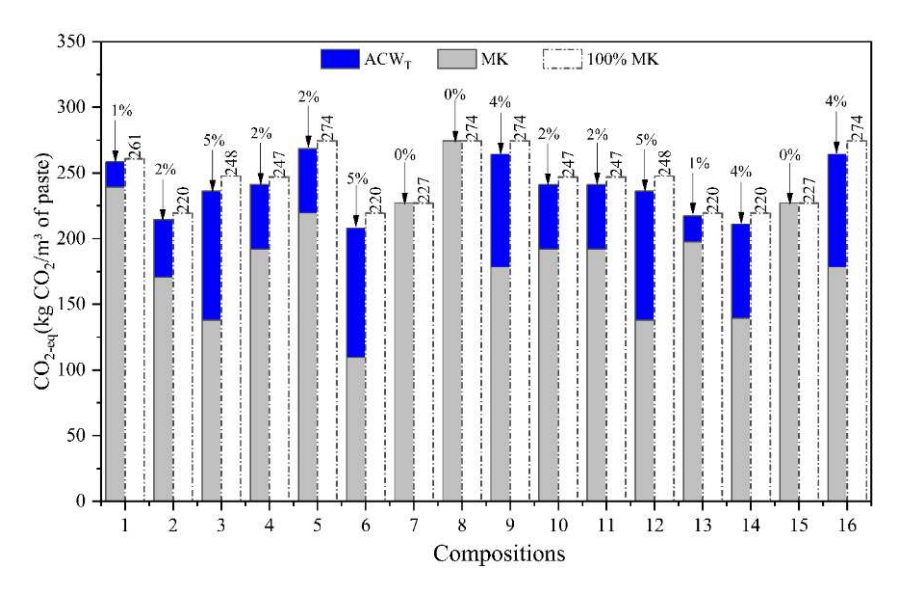


Fig. 9 – Comparison of emissions associated with precursors if only MK is used.

Ruviaro et al. [40] produced geopolymers with up to 20% oat hull ash (OHA) in replacement of MK. The authors reported that the maximum total reductions in ECO<sub>2-eq</sub> were 1%, but the embodied energy and costs decreased by 39% and 24%, respectively. When compared only to MK, OHA had ECO<sub>2-eq</sub> ~15% lower. In another study, Ruviaro et al. [33] evaluated the influence of up to 20% wood ash in the replacement of MK for geopolymer production. Again, ECO<sub>2-eq</sub> reductions were practically insignificant (~0.6%), but when comparing the precursor materials' ECO<sub>2-eq</sub>, wood ashes showed reductions of ~69% compared to MK. In both studies, authors reported that the total ECO<sub>2-eq</sub> was not significant because the activators (NaOH and KOH) had a high environmental burden, dominating the equivalent emissions in geopolymer systems, as occurred in this study. In contrast, in Portland cement-based systems, where supplementary cementitious materials and/or waste materials end up replacing the component with the highest environmental impact, Portland cement results in significant ECO<sub>2-eq</sub> reductions.

Finally, regarding the environmental analysis related to CO<sub>2</sub> emissions, even though the reductions were small with the partial replacement of MK by ACW<sub>T</sub>, the valorization and inertization of waste materials containing asbestos are of great environmental and, primarily, social interest, as asbestos fibers are responsible for numerous serious illnesses and soil and water contamination [41,42].

### 3.1. Rheological analyzes

After the dissolution of silicates and aluminosilicates by mixing the activator solution with the precursor material, microstructure development occurs through the condensation of the monomeric units. This reaction process affects the rheology of the mixtures and is influenced by the characteristics of the components used. Although the rheological behavior of geopolymer mixtures based on metakaolin is already known, the presence of a second precursor rich in calcium in the system can modify this behavior.

In this sense, Fig. 10a and Fig. 10b show the behavior of the flow curves (viscosity and shear stress versus shear rate) for the alkali-activated matrices produced with metakaolin, ACW<sub>T</sub>, and liquid sodium silicate (LSS). It can be observed that all evaluated formulations exhibit the same behavior of increasing shear stress and decreasing equivalent viscosity with increasing shear rate. Similar behavior has been reported in the

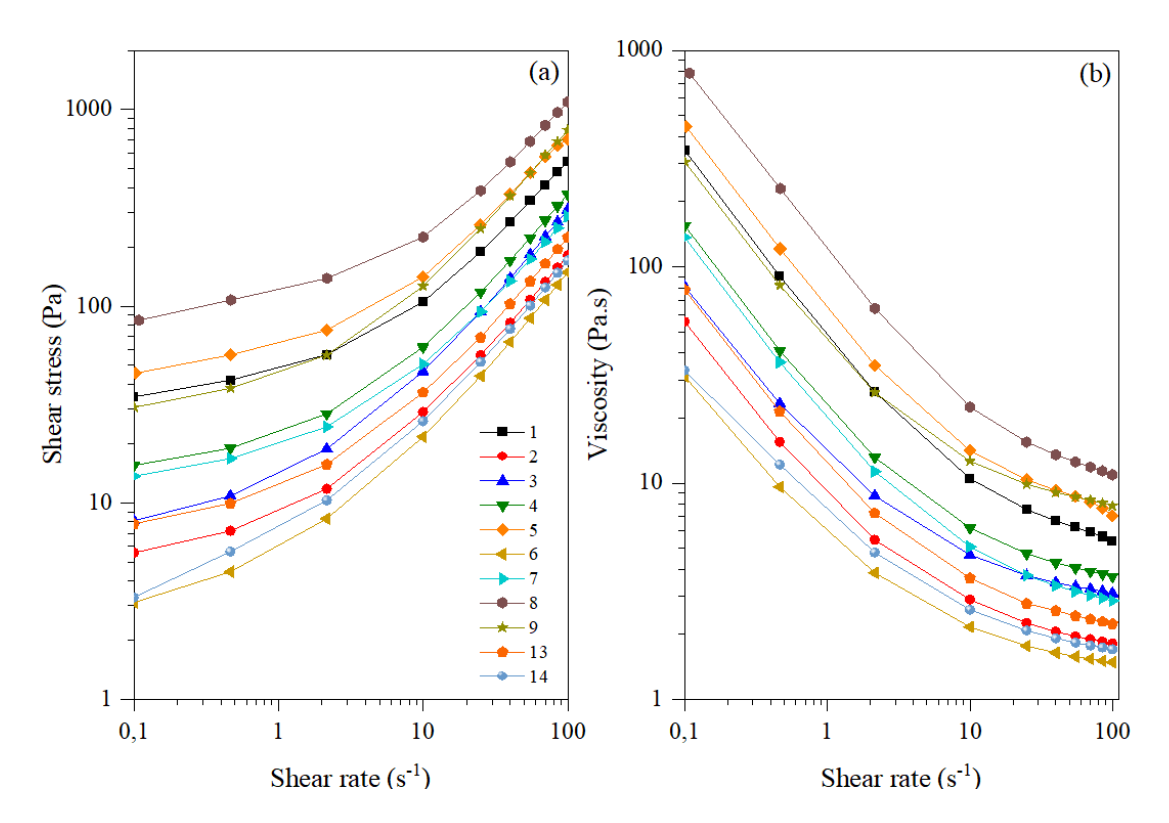


Fig. 10 – Shear stress versus shear rate (a) and equivalent viscosity versus shear rate (b) curves of alkali-activated matrices produced with LSS.

It is noteworthy that the curves for formulations F1, F5, F8, and F9, which exhibit the highest viscosity and shear stress values, are the formulations with the lowest LSS/(ACW<sub>T</sub>+MK) ratio. In other words, these mixtures required higher torque to overcome friction and rotate the rheometer. Strong negative linear correlations of viscosity and yield stress with the mass fraction of the activating solution (-0.95 and -0.83, respectively) were identified. According to Santana et al. [18], mixtures with a higher proportion of the available activating solution exhibit less viscosity due to less friction between particles. Additionally, Lu et al. [14] indicate that the activating solution is the most effective component in the rheological properties of alkali-activated binders.

Fig. 11a and Fig. 11b show the behavior of the flow curves (viscosity and shear stress versus shear rate) for alkali-activated matrices based on liquid potassium silicate (LKS). It can be observed that some formulations exhibit a change in curve behavior,

with an increase in viscosity for high shear rates (F3, F4, F5, F6, F9, and F14), indicating a change in rheological behavior caused by rapid alkali-activation reaction. This behavior was not observed in formulations activated by LSS.

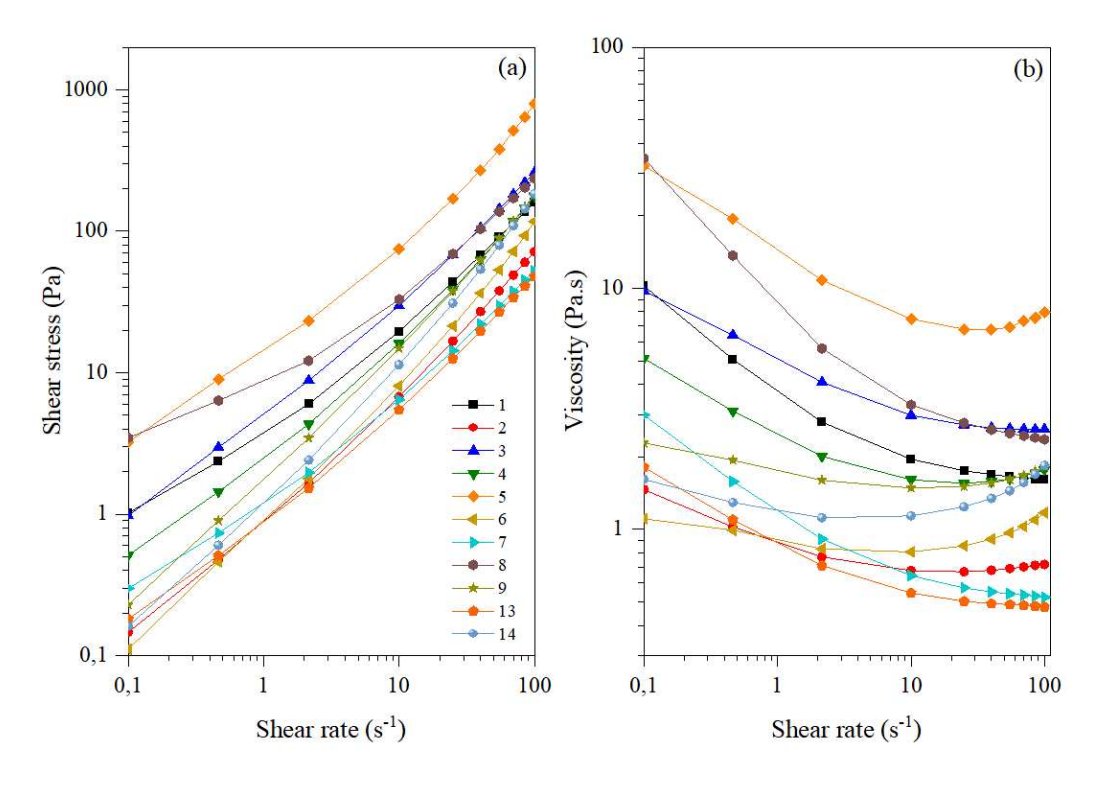


Fig. 11 – Shear stress versus shear rate (a) and equivalent viscosity versus shear rate (b) curves of alkali-activated matrices produced with LKS.

The blends that exhibited anomalous flow curves are composed of higher content of ACW<sub>T</sub>, which consists of 30.63% belite and 27.12% calcite. Belite may have promoted the formation of C-S-H and portlandite, driven by the high alkalinity of the mixture. Calcite, on the other hand, has a surface that favors nucleation and growth of hydrated calcium silicate gel at early ages, accelerating and amplifying the hydration of silicates [45]. For fly ash-based alkali-activated cement (Class C), Yip and Van Deventer [46] and Yip et al. [47] indicated that the setting time and rheological properties of the mixtures were significantly altered by calcium-based compounds through heterogeneous nucleation effects. Additionally, these authors highlighted that a small amount of CaCO<sub>3</sub> reduced the setting time of the mixtures.

According to Park et al. [13], the initial setting time of calcium-free geopolymer binders is generally 12 to 24 hours. Upon introducing calcium into the system, the initial setting time is reduced due to the rapid formation of products involving calcium. Incorporating 30% to 40% of ground-granulated blast-furnace slag reduced the initial setting time of geopolymer binders by 40 minutes [13]. Antoni et al. [48] point out that the use of fly ash with high calcium content can cause a flash set, with insufficient time to use the mixtures in real applications. The authors mentioned that the mixtures might harden in just 5 minutes, consistent with the behavior observed in this study.

According to Antoni et al. [49], calcium-based precursors with fly ash have the advantage of developing stronger matrices due to the coexistence of polymerization and hydration reactions. However, the authors associate the flash set with the pH of the mixture, which is also directly related to the calcium content of the precursor. Furthermore, according to Wijaya et al. [49], a mixture of 20% precursor with 80% distilled water by mass, with a pH above 11, has a high possibility of hardening before 5 minutes. The mixture of ACW<sub>T</sub> with distilled water in the same proportions had a pH of 13.62.

In general, the rapid dissolution of  $Al_2O_3$  and  $SiO_2$  in high pH environments promotes rapid reactions of silicates and aluminates with  $Ca^{2+}$ , producing C-A-S-H and C-S-H, thereby reducing the time of initial and final setting. The reactions of  $Al_2O_3$ ,  $SiO_2$ , and  $Ca^{2+}$  continue until all  $Ca^{2+}$  is consumed. Indeed, it was observed that formulations with higher ACW<sub>T</sub> ratios (F3, F6, and F9) hardened completely after the rheometer test, around 8 minutes after mixing the components.

There are no studies in the literature that correlate the flash set with the type of activator (Na or K). A hypothesis to justify the occurrence of flash set only in mixtures produced with LKS may be the greater ease in the dissolution of Ca<sup>2+</sup> of ACW<sub>T</sub> promoted by the potassium-based activator solution. According to Fig. 12, LKS has lower viscosity than LKS, accelerating the contact of the precursor particles with the k<sup>+</sup> ions and the alkali-activation reactions. The rheological factors were determined by fitting flow curves to Herschel-Bulkley models, applied for silicate-activated alkali mixtures [14, 50].

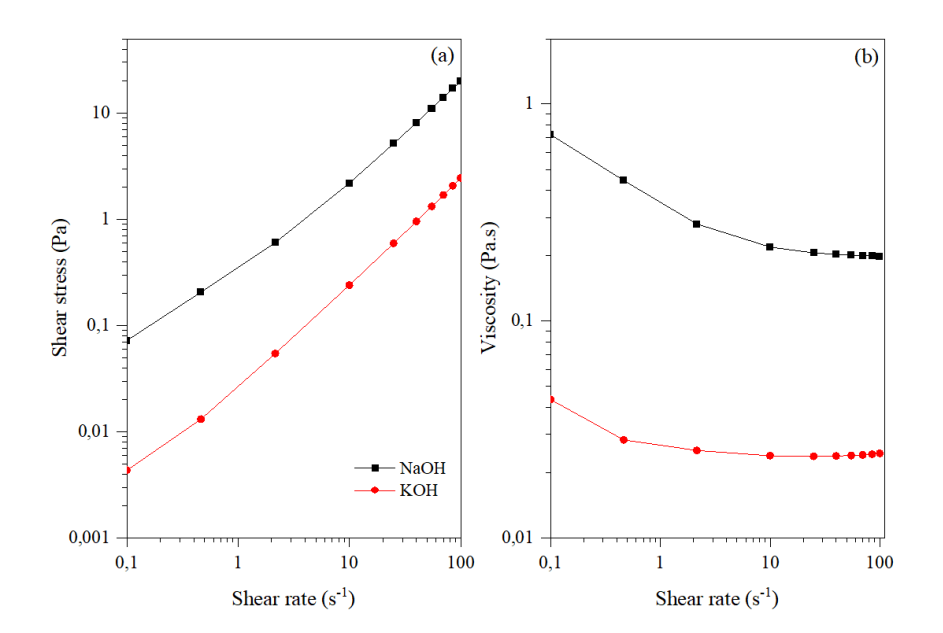


Fig. 12 – Shear stress versus shear rate (a) and equivalent viscosity versus shear rate (b) curves of alkali-activated mixtures produced with LSS and LKS.

It is observed that the LKS presented lower equivalent viscosity and yield stress than the LSS. Fig. 13 presents the plastic viscosities determined for the maximum shear rate equal to 100s-1. The formulations produced with potassium silicate showed values lower than those observed in those produced with sodium silicate. In fact, the difference was promoted by the lower viscosity of the LKS.

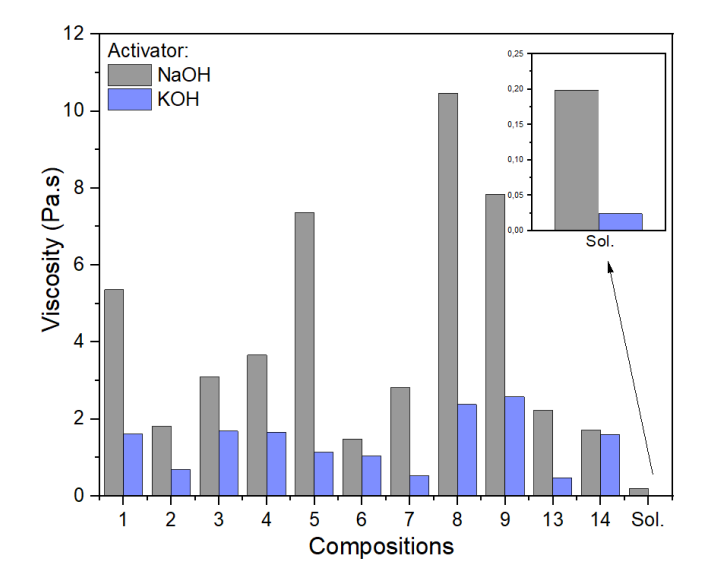


Fig. 43 – Plastic viscosities determined for the maximum shear rate (100 s<sup>-1</sup>) of formulations produced with LSS and LKS.

Vance et al. [51] also identified that matrices activated with NaOH solution generally exhibit higher yield stress and plastic viscosity than matrices based on KOH. According to Poulesquen et al. [52] and Lu et al. [14], this behavior is due to the lower charge density of K<sup>+</sup>, which provides a lower ion-dipole force and, consequently, lower viscosity of the solution. Comparatively, the concentration of Na<sup>+</sup> cations adsorbed on the surface of negatively charged particles is lower than the concentration of K<sup>+</sup>. According to Lu et al. [14], the greater adsorption of K<sup>+</sup> cations can reduce van der Waals forces and increase the repulsive force of the double layer between charged particles, reducing the yield stress of the mixtures. In addition, Na<sup>+</sup> cations tend to combine more easily with free water [14].

### 3.2. Phase formation

The diffractograms of the LSS- and LKS-activated pastes, along with the identified mineral phases, are presented in Fig. 14 and Fig. 15, respectively.

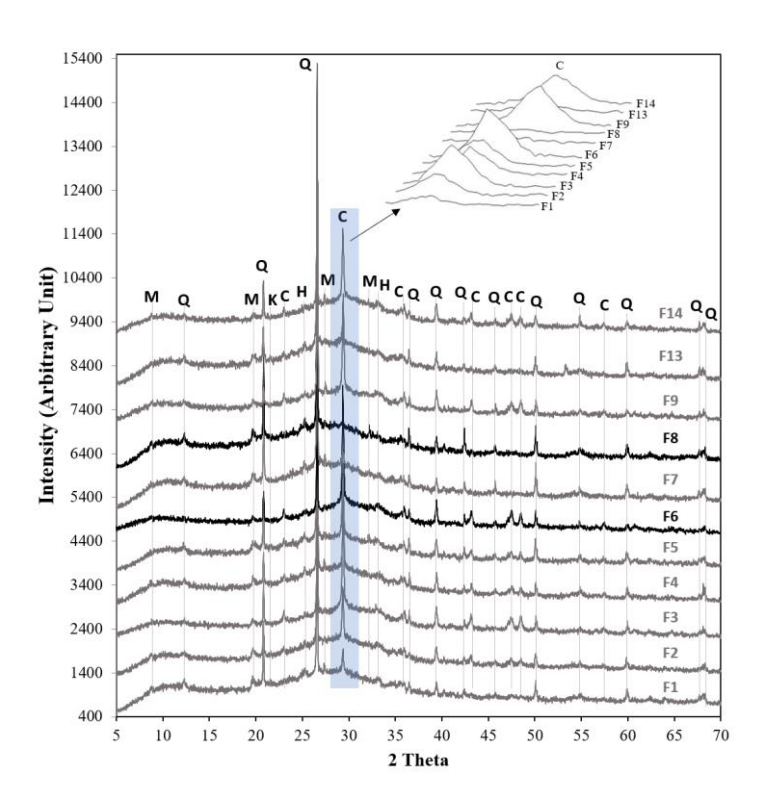


Fig. 54 – Crystal phases identified for pastes produced with LSS. M - muscovite, Q - quartz, K - kaolinite, H - hematite, and C - calcite.

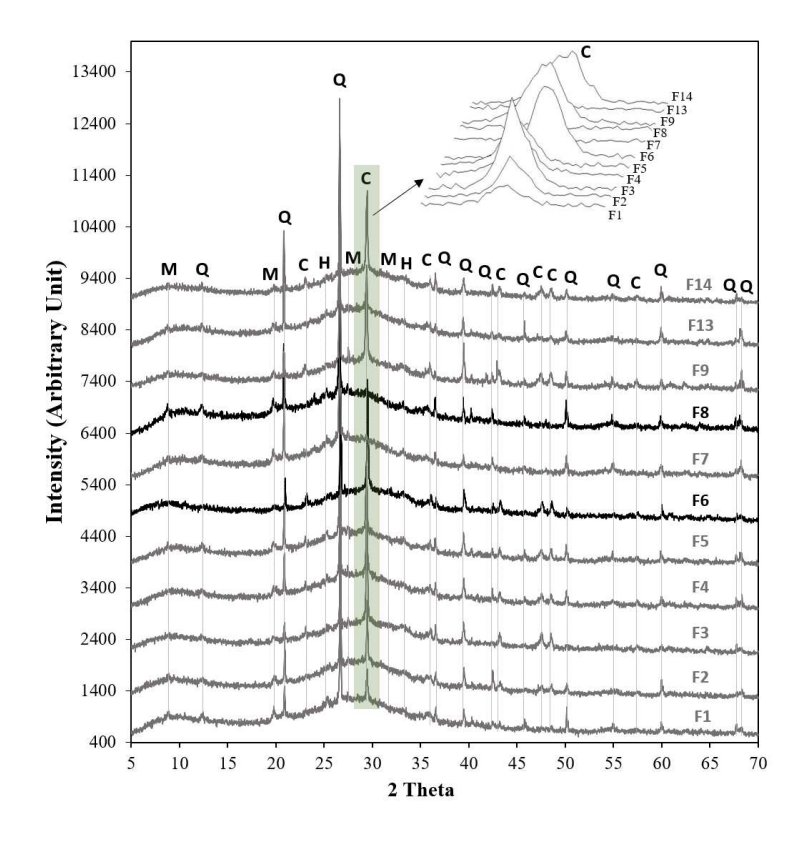


Fig. 65 – Crystalline phases identified for pastes produced with LKS. Being M - muscovite, Q - quartz, K - kaolinite, H - hematite and C - calcite.

The diffractograms revealed the presence of muscovite  $[KAl_2(AlSi_3O_{10})(F,OH)_2]$ , quartz  $(SiO_2)$ , hematite  $(Fe_2O_3)$ , and kaolinite  $[Al_2Si_{25}(OH)_4]$  in all series, which are unreacted phases originating from metakaolin [16]. Additionally, the peaks of calcite  $(CaCO_3)$ , with intensity proportional to calcite content, were identified in most of the series, except for formulations F7, F8, and F15 which do not contain  $ACW_t$  in their composition. In the pastes with  $ACW_T$ , more intense peaks of calcite  $(CaCO_3)$  were identified in mixtures with higher content of this phase.

No belite peaks were identified in the pastes. Furthermore, the absence of portlandite, which typically forms upon belite hydration, was observed. The absence of new crystalline phases containing calcium suggests that CaO may have become part of the amorphous compounds, such as hydrated calcium silicate (C-S-H) or hydrated calcium aluminosilicate (C-A-S-H) [46]. Alternatively, Ca(OH)<sub>2</sub> may have formed in ACW<sub>T</sub>-containing pastes but underwent carbonation.

Carneiro et al. [3] identified portlandite and AFm (monocarboaluminate and hemicarboaluminate) for pastes based on ACW<sub>T</sub> and water. The absence of these phases

in the binary system (metakaolin and  $ACW_T$ ) may be related to the preferential reaction of CaO with the decomposed aluminosilicates from metakaolin to form C-A-S-H and C-S-H.

As reported by Provis et al. [53], the main products of reactions in geopolymer systems are typically amorphous and can be identified by an amorphous halo between  $2\theta=28^{\circ}$  and  $2\theta=30^{\circ}$ . Interestingly, the use of ACW<sub>T</sub> in the pastes caused a displacement of the amorphous halo towards higher angles, as shown in Figure 16. This phenomenon is particularly evident in a comparative analysis of formulations F6 (containing 40% substitution of ACW<sub>T</sub> for metakaolin by mass) and F8 (without ACW<sub>T</sub>). The displacement of the amorphous halo may indicate the formation of C-A-S-H and C-S-H with the inclusion of a calcium-rich material in the system [54]. Furthermore, the formation of C-A-S-H may have occurred preferentially instead of (N, K)-A-S-H, potentiated by the calcium present in ACW<sub>T</sub>.



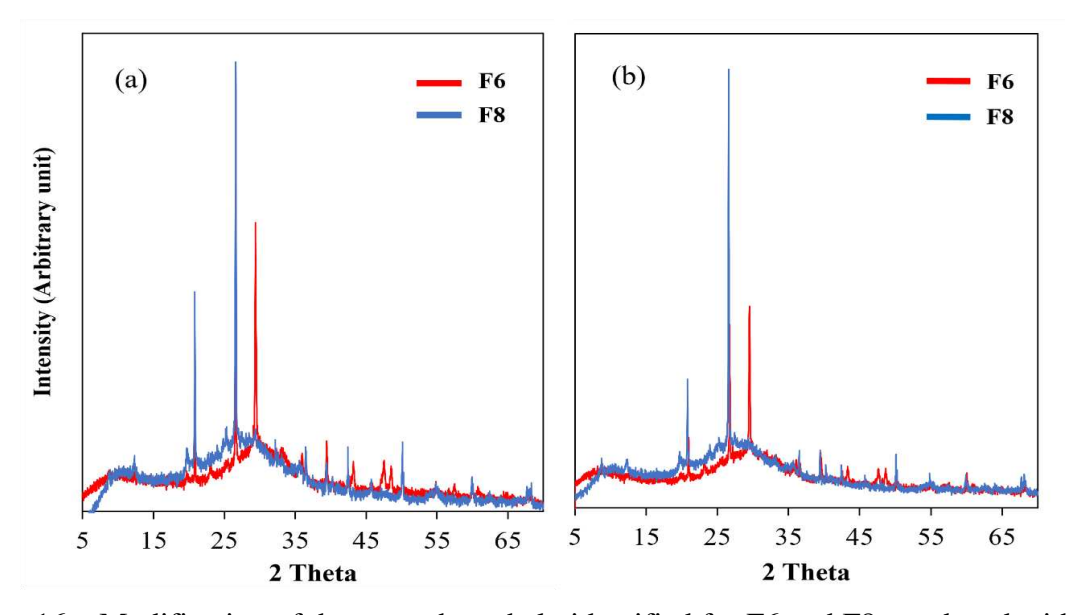


Fig. 16 – Modification of the amorphous halo identified for F6 and F8, produced with a) LSS and b) LKS.

The results indicate that the alkaline activator type did not induce significant changes in the mineralogical phases formed. In contrast, the most important effect was observed upon including a calcium-rich material, which significantly modified the geopolymer phase assemblage.

### 3.3. Compressive strength

Fig. 17 shows the compressive strength behavior of pastes produced with LSS and LKS. It can be observed that the type of activator does not seem to influence the compressive strength, considering that both pastes exhibit the same behavior for this property.

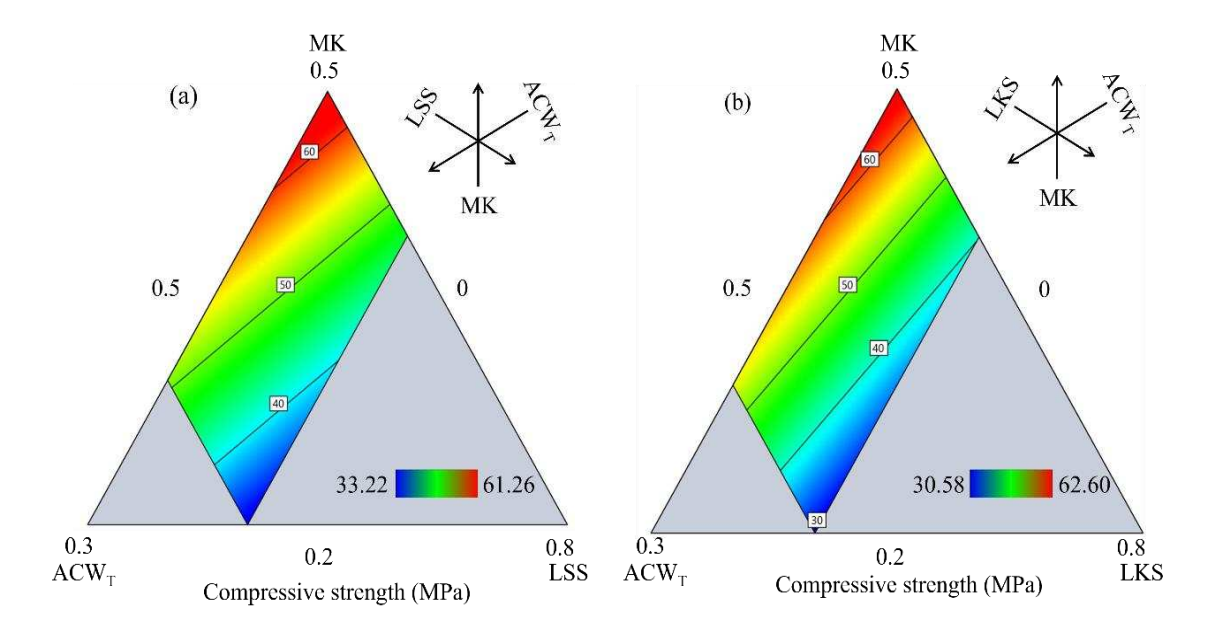


Fig. 17 – Compressive strength of pastes produced with LSS and LKS.

The results show that, independently of the activator nature, an increase in compressive strength occurs with an increase in the mass fraction of metakaolin and a decrease in the mass fraction of the activating solution. The Solution/(ACW<sub>T</sub>+MK) ratio presented an influence on compressive strength analogous to the water/cement ratio in Portland cement-based pastes through distinct mechanisms. In addition to F8, formulations F1, F5, F9, and F16, with low Solution/(ACW<sub>T</sub>+MK) ratios, presented the highest strengths. This behavior is in accordance with consolidated geopolymer reaction models [55] and with results observed in the literature [18], indicating that after the dissolution of aluminosilicates, uncombined water is released from the mixture, forming pores in the matrix that may compromise mechanical performance.

According to the statistical analysis of Cox and Piepel [56] effects, it is noted that the mass fractions of metakaolin and activator solution have a significant effect on compressive strength ( $\alpha = 0.05$ ). On the other hand, ACW<sub>T</sub> had no significant effect ( $\alpha = 0.05$ ) on the compressive strength of the mixtures.

Although part of the CaO contained in  $ACW_T$  is expected to promote the formation of new products, such as C-A-S-H and C-S-H [46], contributing to the compressive strength, the replacement of metakaolin (a more reactive material) may have reduced the formation of N-A-S-H, compensating the formation of new products. Additionally, the addition of material rich in calcite (more than 20% by mass) in an alkaliactivated mixture can cause structural discontinuity and matrix shrinkage [46]. Formulation F6, with a higher mass fraction of  $ACW_T$ , contains 13.56% of calcite.

Furthermore, for the formulations produced with LKS that presented lower compressive strengths (F2, F6, F13, and F14), it was observed that the samples cracked when immersed in water during the determination of electrical conductivity, leading to complete deterioration. A plausible hypothesis is that potassium silicate may be refining the pores of the matrices and that the tensile strength of these formulations may be inferior to the capillary tension at the initial moment of immersion.

Fig. 18 presents the ECO<sub>2-eq</sub> intensity (IC) for the LSS- and LKS-activated pastes are presented. IC was obtained by the ratio between greenhouse gas equivalence in carbon dioxide (kg CO<sub>2</sub>/m<sup>3</sup> paste) and compressive strength values (MPa), being an important parameter to simultaneously evaluate the mechanical and environmental performance of the material.

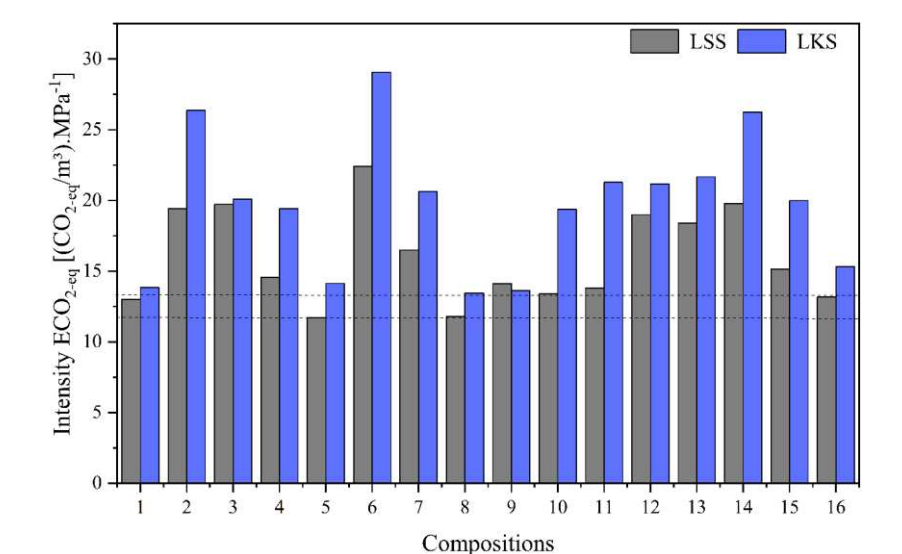


Fig. 18 – ECO<sub>2-eq</sub> intensity for compositions activated by LSS and by LKS.

Thus, for the NaOH activator, the composition with the lowest IC is F5, and for KOH, it is F8, with values of 11.71 and 13.45 (kg CO<sub>2-eq</sub>/m³).MPa<sup>-1</sup>, respectively. This is due to the good mechanical performance of the compositions and the low ECO<sub>2-eq</sub> emissions of these matrices. As expected, compositions with higher activator contents (2, 6, 13, and 14) presented higher ICs, due to the higher CO<sub>2</sub> emissions from the activators, as previously shown.

# 3.3. Analysis of free alkalis

To evaluate the influence of the alkali activator base (Na and K) and ACW<sub>T</sub> on dosage efficiency, the mass of efflorescence extracted from the geopolymer samples and the electrical conductivity of distilled and deionized water of the residual solution after sample immersion were evaluated. Fig. 19 and Fig. 20 present ternary diagrams showing the influence of the components of the paste on the mass of efflorescence determined for the formulations produced with LSS and LKS. Additionally, for each formulation, the geopolymeric samples, after the leaching of free alkali ions in the form of efflorescence, are presented.

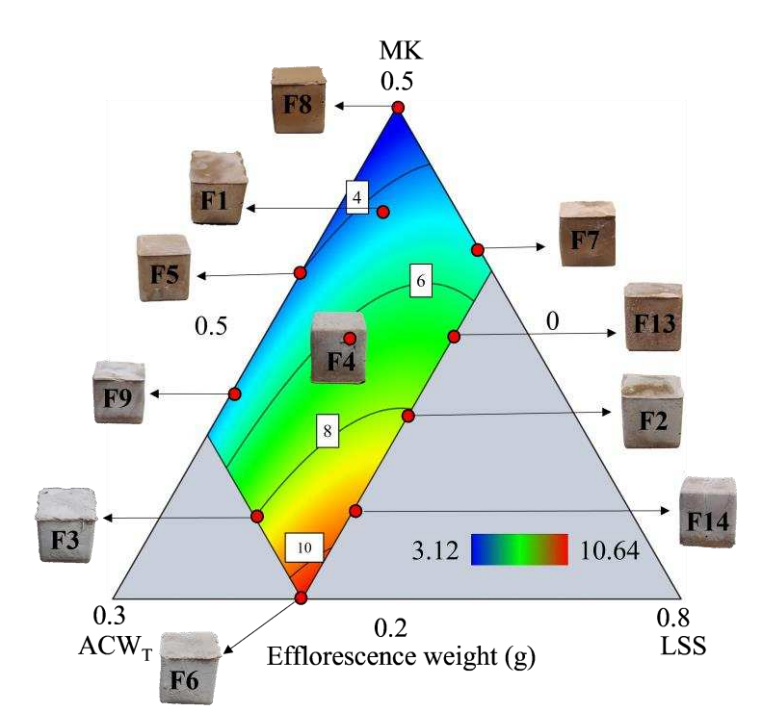


Fig. 19 – Ternary diagram for the efflorescence mass of formulations produced with LSS.

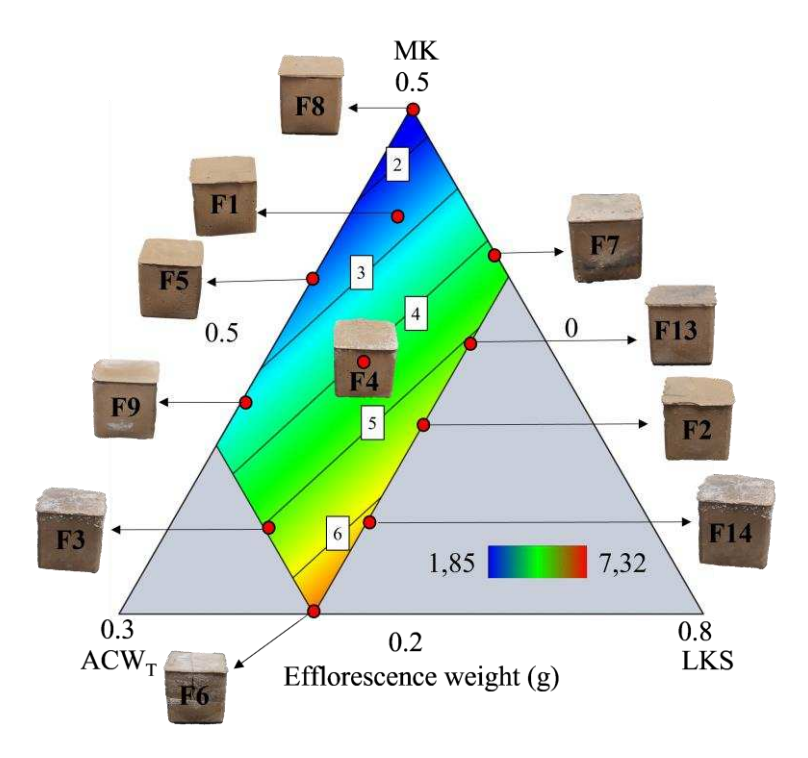


Fig. 20 – Ternary diagram for the efflorescence mass of formulations produced with LKS.

It is noted that, for both evaluated systems, there is an increase in efflorescence mass when the mass fraction of the activating solution is increased or by increasing the Solution/(ACW<sub>T</sub>+MK) ratio. Observing the extreme points of the diagram, the manifestation of efflorescence on the surface of the F6 samples (whitish appearance) is not observed in F8. Formulation F6 has a Na<sub>2</sub>O/Al<sub>2</sub>O<sub>3</sub> ratio of 1.79 and K<sub>2</sub>O/Al<sub>2</sub>O<sub>3</sub> ratio of 1.46, while for F8 the ratio is 0.66 for LSS and 0.54 for LKS. The optimal ratio for balancing the negative charge of Al<sup>-</sup> with the cations Na<sup>+</sup> or K<sup>+</sup>, avoiding free alkali ions in the matrix, is equal to 1 [20]. However, some factors, such as component reactivity and paste rheology, can make it difficult to use the appropriate (Na, K)<sub>2</sub>O/Al<sub>2</sub>O<sub>3</sub> ratio [18].

Despite the similar behavior of the pastes produced with LSS and LKS, the efflorescence mass values for the pastes produced with LKS are considerably lower. According to Poulesquen [52], potassium-based activated solutions have a stronger base than sodium-based solutions. According to the authors, the ionization rate varies with the basicity of the alkali ion, where K<sup>+</sup> is superior to Na<sup>+</sup>. Kani et al. [57] also highlighted that geopolymers based on potassium are less susceptible to efflorescence formation due to the strong bond of potassium within the alkali aluminosilicate gel framework. In addition, potassium carbonate crystals are less visible than sodium carbonate [57].

Fig. 21a shows the electrical conductivity values of the residual solution for the formulations produced with LSS and LKS, and Fig. 21b highlights the strong correlation between the electrical conductivity and compressive strength of the evaluated pastes.

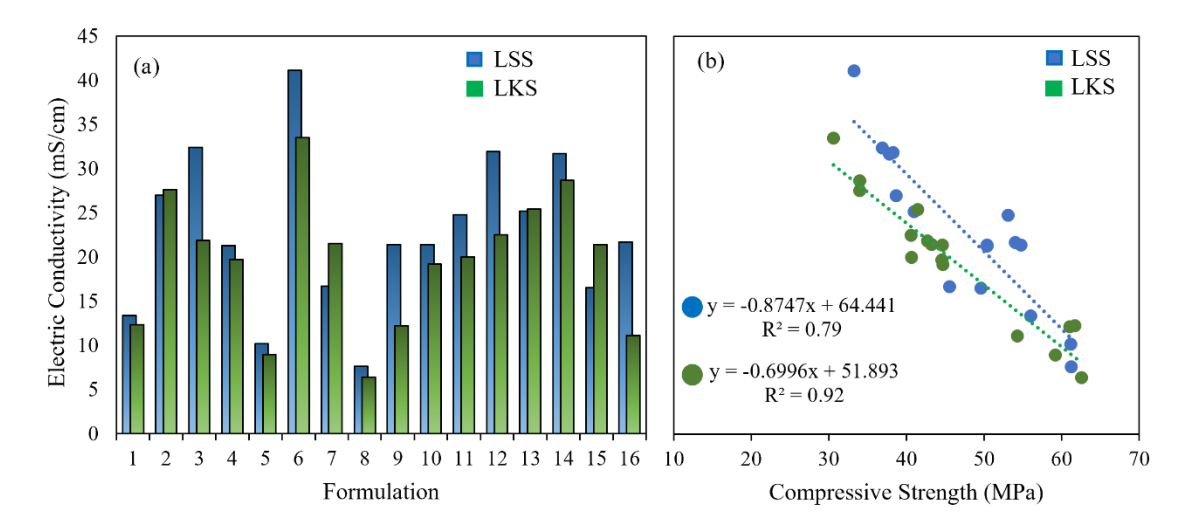


Fig. 21 – (a) Electrical conductivity of formulations produced with LSS and LKS and (b) correlations between compressive strength and electrical conductivity.

This correlation was already expected, as the efflorescence deposited on the surface of the geopolymer samples is composed of sodium or potassium carbonate [(Na, K)<sub>2</sub>CO<sub>3</sub>], and when samples containing Na<sub>2</sub>CO<sub>3</sub> are submerged in water, this compound dissociates into 2Na<sup>+</sup> or 2K<sup>+</sup> and CO<sub>3</sub>-<sup>2</sup>. The increase in free electrons in the solution increases electrical conductivity. The excess of free ions, indirectly quantified by electrical conductivity, indicates that the proportions of the formulation components are not adequate and directly impact other properties of the paste, as observed in F6, which in addition to low compressive strength and high mass of efflorescent material on the sample surfaces, presents the highest electrical conductivity for both evaluated systems.

According to the analysis of the Cox and Piepel effects [56], it is inferred for the pastes produced with LSS that the ACW<sub>T</sub> does not have a significant influence on electrical conductivity ( $\alpha = 0.05$ ), that is, replacing metakaolin with ACW<sub>T</sub> seems not to modify the fixation of alkalis in the products formed during the geopolymer formation reactions. On the other hand, for pastes produced with LKS, the analysis of the effects showed that increasing the mass fraction of ACW<sub>T</sub> has a significant influence ( $\alpha = 0.05$ ) on reducing electrical conductivity. Probably, LKS has greater efficiency in decomposing

components of ACW<sub>T</sub>, such as CaO, which may be fixing alkalis during the formation of new alkali-activated products.

# 3.4 Simultaneous optimization and model validation

To determine formulations of geopolymer mixtures that simultaneously meet performance, aesthetics and sustainability parameters, prediction models were determined. The models, obtained through Scheffé's linear polynomial, correlate the properties with the mass fractions of the components.

Equation 7 ( $R^2_{adj}$ = 1.0 and  $R^2_{pred}$ = 1.0) and Equation 8 ( $R^2_{adj}$ = 1.0 and  $R^2_{pred}$ = 1.0) are the models for greenhouse gas equivalence in carbon dioxide (ECO<sub>2-eq</sub>) of the mixtures activated with LSS and LKS, respectively.

$$ECO_{2-eq} = 548.83MK + 491.24ACW_T + 894.99LSS$$
 (Eq. 7)

$$ECO_{2-eq} = 548.83MK + 491.17 + 1135.13KS$$
 (Eq. 8)

Equation 9 ( $R^2_{adj}$ = 0.85 and  $R^2_{pred}$ = 0.82) and Equation 10 ( $R^2_{adj}$ = 0.90 and  $R^2_{pred}$ = 0.88) are the models for compressive strength ( $C_s$ ) of the mixtures activated with LSS and LKS, respectively.

$$C_s = 158.26MK + 89.93ACW_T - 28.99LSS$$
 (Eq. 9)

$$C_s = 186.96MK + 134.57ACW_T - 57.72LKS$$
 (Eq. 10)

Equation 11 ( $R^2_{adj}$ = 0.95 and  $R^2_{pred}$ = 0.93) and Equation 12 ( $R^2_{adj}$ = 0.99 and  $R^2_{pred}$ = 0.98) are the models for electrical conductivity values ( $\sigma$ ) of the mixtures activated with LSS and LKS, respectively.

$$\sigma = -69.55MK + 27.24ACW_T + 79.24LSS$$
 (Eq. 11)

$$\sigma = -87.59MK - 50.23ACW_T + 99.16LKS$$
 (Eq. 12)

To determine a formulation that simultaneously incorporates all desired characteristics for geopolymers, the Design-Expert® software was used based on the desirability function developed by Derringer and Suich (1980). The objective was to determine for each activator (LSS and LKS) a formulation that would simultaneously minimize the equivalence of greenhouse gas in carbon dioxide and electrical conductivity and maximize compressive strength and consumption of ACW<sub>T</sub>.

According to the simulation in Design-Expert® software, the optimized formulation for sodium silicate-based pastes presents a mass fraction of MK equal to 0.345, ACW<sub>T</sub> equal to 0.155, and LSS equal to 0.500. For potassium silicate-based paste, the optimal formulation presents a mass fraction of MK equal to 0.300, ACW<sub>T</sub> equal to 0.200, and LKS equal to 0.500. The predicted values for each formulation, confidence limits, observed experimental values, and the deviation between the observed and predicted values by the models are presented in Table 6.

Table 6 – Predicted and experimentally observed values for optimized formulations produced with LSS and LKS

Activator	Property	Predicted by the model	Lower limit (α=0.05)	Upper limit (α=0.05)	Experimental result
	ECO <sub>2-eq</sub>	712.97	712.96	712.98	712.97
LSS	$C_S$ (MPa)	54.03	50.68	57.38	51.12
	Ce(mS/cm)	19.86	17.90	21.82	21.96
	ECO <sub>2-eq</sub>	830.44	830.43	830.44	830.44
LKS	$C_S$ (MPa)	54.14	50.43	57.85	56.44
	Ce (mS/cm)	13.26	12.30	14.22	12.32

It is noted that the established models were efficient in predicting the properties, making it possible to determine formulations of geopolymer pastes with the incorporation of a residue, presenting high compressive strength, and reducing efflorescence (observed indirectly by electrical conductivity) and CO<sub>2</sub> emissions.

Also, it is observed that under the same established conditions, the formulation optimized with potassium silicate allowed greater incorporation of ACW<sub>T</sub> than the formulation established with sodium silicate, probably due to the greater efficiency of potassium in the decomposition of precursor materials. On the other hand, the production

of a potassium silicate-based binder has a greater carbon footprint, justified by the greater contribution of KOH to polluting gas emissions and consumption in its production cycle.

### 4. CONCLUSIONS

It was proposed to evaluate the influence of  $ACW_T$  and the alkaline activator (Na or K) on the properties of fresh and hardened geopolymer matrix, as well as the associated pollutant gas emissions.

Environmental analysis showed that mixtures produced based on potassium contain a higher  $CO_2$  footprint. In addition, the insertion of  $ACW_T$  reduces the  $CO_{2\text{-eq}}$  associated with the formulations, as well as enabling the inertization and proper disposal of hazardous waste.

According to rheological analyses, it was noted that for both alkaline activators used, the increase in the activating solution promotes a reduction in viscosity and yield stress by reducing the friction between particles that have not yet been diluted. Only for the formulations activated with potassium silicate and with a higher proportion of ACW<sub>T</sub> (a source of calcium), a rapid increase in viscosity occurred for high shear rates with a reduction in the setting time. This behavior may be associated with the greater ease of potassium silicate in decomposing Ca<sup>2+</sup> ions from calcite with the formation of C–A–S–H and the hydration of belite, forming C–S–H.

Although LKS accelerated the reactions of pastes with ACW<sub>T</sub>, this effect was not significant in phase formation, probably due to the analysis being performed at 28 days. The absence of belite was observed for both alkaline activators, which may have hydrated and formed some non-crystalline product. In addition, some of the calcium present in calcite may have reacted, forming C–S–H and C–A–S–H, a hypothesis consistent with the modification of the amorphous halo in the XRD data.

Similar to the water/cement ratio in Portland cement matrices, the proportion of the activating solution governed the compressive strength of the matrices with the two activators used. In fact, excess liquid released during geopolymer reaction and formation can increase porosity and decrease mechanical performance.

Through the analysis of free alkalis, it was noted that K<sup>+</sup> ions are more strongly bound in the alkali aluminosilicate gel structure of the geopolymer samples, and the

737	matr	ices produced with LKS showed less efflorescence and lower electrical conductivity
738	of th	e leached solution. A strong linear correlation was also observed between electrical
739	cond	luctivity and compressive strength, probably due to the dependence of these two
740	varia	ables on the proportion of the same component, the activating solution.
741		
742	ACI	KNOWLEDGMENTS
743		The authors would like to acknowledge the financial support of CNPq (Process no
744	3092	270/2022-7) and FAPESB (Process n° 687/2020).
745		
746	DEC	CLARATION OF COMPETING INTEREST
747		The authors declare that they have no known competing financial interests or
748	perso	onal relationships that could have appeared to influence the work reported in this
749	pape	r.
750		
751	REF	TERÊNCIAS
752	[1]	A. Godono, M. Clari, N. Franco, C. Ciocan, I. Mansour, C. Zunarelli, E. Pira, P.
753		Boffetta, The association between occupational asbestos exposure with the risk of
754		incidence and mortality from prostate cancer: a systematic review and meta-analysis,
755		Prostate Cancer Prostatic Dis. 2021 254. 25 (2021) 604-614.
756		https://doi.org/10.1038/s41391-021-00437-x.
757	[2]	L. Stayner, L.S. Welch, R. Lemen, The Worldwide Pandemic of Asbestos-Related
758		Diseases, Https://Doi.Org/10.1146/Annurev-Publhealth-031811-124704. 34 (2013) 205-
759		216. https://doi.org/10.1146/ANNUREV-PUBLHEALTH-031811-124704.
760	[3]	G.O. Carneiro, T.A. Santos, G. Simonelli, D. V. Ribeiro, M.S. Cilla, C.M.R. Dias,
761		Thermal treatment optimization of asbestos cement waste (ACW) potentializing its use
762		as alternative binder, J. Clean. Prod. 320 (2021) 128801.
763		https://doi.org/10.1016/J.JCLEPRO.2021.128801.
764	[4]	L. Tomassetti, D. Di Giuseppe, A. Zoboli, V. Paolini, M. Torre, E. Paris, E. Guerriero, F.
765		Petracchini, A.F. Gualtieri, Emission of fibres and atmospheric pollutants from the
766		thermal treatment of asbestos containing waste (ACW), J. Clean. Prod. 268 (2020)

 $122179.\ https://doi.org/10.1016/J.JCLEPRO.2020.122179.$ 

- 768 [5] Y. Yvon, P. Sharrock, Characterization of thermochemical inactivation of asbestos
- containing wastes and recycling the mineral residues in cement products, Waste and
- 770 Biomass Valorization. 2 (2011) 169–181. https://doi.org/10.1007/S12649-011-9063-
- 771 9/FIGURES/5.
- 772 [6] T.A. Santos, M.S. Cilla, e D. V. Ribeiro, Use of asbestos cement tile waste (ACW) as
- mineralizer in the production of Portland cement with low CO2 emission and lower
- energy consumption, J. Clean. Prod. 335 (2022) 130061.
- 775 https://doi.org/10.1016/J.JCLEPRO.2021.130061.
- 776 [7] A.F. Gualtieri, M. Boccaletti, Recycling of the product of thermal inertization of
- cement–asbestos for the production of concrete, Constr. Build. Mater. 25 (2011) 3561–
- 778 3569. https://doi.org/10.1016/J.CONBUILDMAT.2011.03.049.
- 779 [8] G.O. Carneiro, H.A. Santana, D. V. Ribeiro, M.S. Cilla, C.M.R. Dias, One-part alkali-
- activated binder produced from inertized asbestos cement waste, J. Clean. Prod. 367
- 781 (2022) 132966. https://doi.org/10.1016/J.JCLEPRO.2022.132966.
- 782 [9] H.A. Santana, N.S.A. Júnior, G.O. Carneiro, D. V. Ribeiro, M.S. Cilla, C.M.R. Dias,
- Asbestos-cement wastes as supplementary precursors of NaOH-activated binders,
- 784 Constr. Build. Mater. 364 (2023) 129921.
- 785 https://doi.org/10.1016/J.CONBUILDMAT.2022.129921.
- 786 [10] Temuujin, j. v.; Van Riessen, a.; Williams, R. Influence of calcium compounds on the
- mechanical properties of fly ash geopolymer pastes. Journal of hazardous materials, v.
- 788 167, n. 1-3, p. 82-88, 2009. https://doi.org/10.1016/j.jhazmat.2008.12.121
- 789 [11] Zhang, Z., Wang, H., Zhu, Y., Reid, A., Provis, J. L., & Bullen, F.. Using fly ash to
- partially substitute metakaolin in geopolymer synthesis. **Applied Clay Science**, v. 88, p.
- 791 194-201, 2014. https://doi.org/10.1016/j.clay.2013.12.025
- 792 [12] Li, F., Liu, L., Yang, Z., & Li, S. Physical and mechanical properties and micro
- characteristics of fly ash-based geopolymer paste incorporated with waste Granulated
- 794 Blast Furnace Slag (GBFS) and functionalized Multi-Walled Carbon Nanotubes
- 795 (MWCNTs). **Journal of Hazardous Materials**, v. 401, p. 123339, 2021.
- 796 https://doi.org/10.1016/j.jhazmat.2020.123339
- 797 [13] S. Park, K.A. Moges, S. Wu, S. Pyo, Characteristics of hybrid alkaline cement
- composites with high cement content: flash set and high compressive strength, J. Mater.
- 799 Res. Technol. 17 (2022) 1582–1597. https://doi.org/10.1016/J.JMRT.2022.01.105.
- 800 [14] C. Lu, Z. Zhang, C. Shi, N. Li, D. Jiao, Q. Yuan, Rheology of alkali-activated materials:
- 801 A review, Cem. Concr. Compos. 121 (2021) 104061.

- https://doi.org/10.1016/J.CEMCONCOMP.2021.104061.
- 803 [15] P. Timakul, W. Rattanaprasit, P. Aungkavattana, Enhancement of compressive strength
- and thermal shock resistance of fly ash-based geopolymer composites, Constr. Build.
- 805 Mater. 121 (2016) 653–658. https://doi.org/10.1016/J.CONBUILDMAT.2016.06.037.
- 806 [16] Telschow, S., Frandsen, F., Theisen, K., & Dam-Johansen, K. Cement Formation A
- Success Story in a Black Box: High Temperature Phase Formation of Portland Cement
- 808 Clinker. **Industrial & engineering chemistry research**, v. 51, n. 34, p. 10983-11004,
- 809 2012. https://doi.org/10.1021/ie300674j
- 810 [17] P. Duxson, J.L. Provis, G.C. Lukey, S.W. Mallicoat, W.M. Kriven, J.S.J. Van Deventer,
- 811 Understanding the relationship between geopolymer composition, microstructure and
- mechanical properties, Colloids Surfaces A Physicochem. Eng. Asp. 269 (2005) 47–58.
- 813 https://doi.org/10.1016/J.COLSURFA.2005.06.060.
- 814 [18] H.A. Santana, J.S. Andrade Neto, N.S. Amorim Júnior, D. V. Ribeiro, M.S. Cilla,
- 815 C.M.R. Dias, Self-compacting geopolymer mixture: Dosing based on statistical mixture
- design and simultaneous optimization, Constr. Build. Mater. 249 (2020) 118677.
- 817 https://doi.org/10.1016/J.CONBUILDMAT.2020.118677.
- 818 [19] K. Gao, K.L. Lin, D. Wang, C.L. Hwang, H.S. Shiu, Y.M. Chang, T.W. Cheng, Effects
- SiO2/Na2O molar ratio on mechanical properties and the microstructure of nano-SiO2
- metakaolin-based geopolymers, Constr. Build. Mater. 53 (2014) 503–510.
- 821 https://doi.org/10.1016/J.CONBUILDMAT.2013.12.003.
- 822 [20] K. Juengsuwattananon, F. Winnefeld, P. Chindaprasirt, K. Pimraksa, Correlation
- between initial SiO2/Al2O3, Na2O/Al2O3, Na2O/SiO2 and H2O/Na2O ratios on phase
- and microstructure of reaction products of metakaolin-rice husk ash geopolymer, Constr.
- 825 Build. Mater. 226 (2019) 406–417.
- 826 https://doi.org/10.1016/J.CONBUILDMAT.2019.07.146.
- 827 [21] W.J. Long, Z. Wu, K.H. Khayat, J. Wei, B. Dong, F. Xing, J. Zhang, Design, dynamic
- performance and ecological efficiency of fiber-reinforced mortars with different binder
- 829 systems: Ordinary Portland cement, limestone calcined clay cement and alkali-activated
- 830 slag, J. Clean. Prod. 337 (2022) 130478.
- https://doi.org/10.1016/J.JCLEPRO.2022.130478.
- 832 [22] T. Stengel, P. Schießl, Life cycle assessment (LCA) of ultra high performance concrete
- 833 (UHPC) structures, Eco-Efficient Constr. Build. Mater. Life Cycle Assess. (LCA), Eco-
- 834 Labelling Case Stud. (2014) 528–564. https://doi.org/10.1533/9780857097729.3.528.
- 835 [23] J. Hong, W. Chen, Y. Wang, C. Xu, X. Xu, Life cycle assessment of caustic soda

- production: a case study in China, J. Clean. Prod. 66 (2014) 113–120.
- https://doi.org/10.1016/J.JCLEPRO.2013.10.009.
- 838 [24] M.A. Villaquirán-Caicedo, R.M. de Gutiérrez, Synthesis of ceramic materials from
- ecofriendly geopolymer precursors, Mater. Lett. 230 (2018) 300–304.
- https://doi.org/10.1016/J.MATLET.2018.07.128.
- 841 [25] Y.K. Kong, K. Kurumisawa, S.H. Chu, Infilled cementitious composites (ICC) A
- comparative life cycle assessment with UHPC, J. Clean. Prod. 377 (2022) 134051.
- 843 https://doi.org/10.1016/J.JCLEPRO.2022.134051.
- 844 [26] R. Bajpai, K. Choudhary, A. Srivastava, K.S. Sangwan, M. Singh, Environmental impact
- assessment of fly ash and silica fume based geopolymer concrete, J. Clean. Prod. 254
- 846 (2020) 120147. https://doi.org/10.1016/J.JCLEPRO.2020.120147.
- 847 [27] D.K. Panesar, K.E. Seto, C.J. Churchill, Impact of the selection of functional unit on the
- life cycle assessment of green concrete, Int. J. Life Cycle Assess. 22 (2017) 1969–1986.
- 849 https://doi.org/10.1007/S11367-017-1284-0/TABLES/8.
- 850 [28] A.S. Ruviaro, G.T.D.S. Lima, M. Taborda-Barraza, L. Silvestro, J.C. Rocha, J. de Brito,
- P.J.P. Gleize, F. Pelisser, Characterization and investigation of the use of oat husk ash as
- supplementary cementitious material as partial replacement of Portland cement: Analysis
- of fresh and hardened properties and environmental assessment, Constr. Build. Mater.
- 363 (2022) (In press). https://doi.org/10.1016/j.conbuildmat.2022.129762.
- 855 [29] H. Pervez, Y. Ali, A. Petrillo, A quantitative assessment of greenhouse gas (GHG)
- emissions from conventional and modular construction: A case of developing country, J.
- 857 Clean. Prod. 294 (2021) 126210. https://doi.org/10.1016/J.JCLEPRO.2021.126210.
- 858 [30] R. Kusiorowski, T. Zaremba, J. Piotrowski, J. Adamek, Thermal decomposition of
- different types of asbestos, J. Therm. Anal. Calorim. 109 (2012) 693–704.
- 860 https://doi.org/10.1007/S10973-012-2222-9.
- 861 [31] M. Lippmann, Toxicological and epidemiological studies on effects of airborne fibers:
- Coherence and public health implications, Crit. Rev. Toxicol. 44 (2014) 643–695.
- https://doi.org/10.3109/10408444.2014.928266.
- P.R. de Matos, R.D. Sakata, P.J.P. Gleize, J. de Brito, W.L. Repette, Eco-friendly ultra-
- high performance cement pastes produced with quarry wastes as alternative fillers, J.
- 866 Clean. Prod. 269 (2020) 122308. https://doi.org/10.1016/j.jclepro.2020.122308.
- 867 [33] L. Silvestro, T.P. Scolaro, A.S. Ruviaro, G.T. dos Santos Lima, P.J.P. Gleize, F. Pelisser,
- Use of biomass wood ash to produce sustainable geopolymeric pastes, Constr. Build.
- 869 Mater. 370 (2023) 130641. https://doi.org/10.1016/J.CONBUILDMAT.2023.130641.

- [34] K. Scrivener, R. Snellings, B. Lothenbach, A Practical Guide to Microstructural Analysis
   of Cementitious Materials, 2018. https://doi.org/10.1201/b19074.
- 872 [35] K. Vance, A. Arora, G. Sant, N. Neithalath, Rheological evaluations of interground and
- blended cement–limestone suspensions, Constr. Build. Mater. 79 (2015) 65–72.
- 874 <a href="https://doi.org/10.1016/J.CONBUILDMAT.2014.12.054">https://doi.org/10.1016/J.CONBUILDMAT.2014.12.054</a>.
- 875 [36] Longhi, M. A., Zhang, Z., Walkley, B., Rodríguez, E. D., & Kirchheim, A. P. Strategies
- for control and mitigation of efflorescence in metakaolin-based geopolymers. **Cement**
- **and Concrete Research**, v. 144, p. 106431, 2021.
- https://doi.org/10.1016/j.cemconres.2021.106431
- 879 [37] F. De Larrard, C.F. Ferraris, T. Sedran, Fresh concrete: A Herschel-Bulkley material,
- 880 Mater. Struct. Constr. 31 (1996) 494–498. https://doi.org/10.1007/bf02480474.
- 881 [38] L.K. Turner, F.G. Collins, Carbon dioxide equivalent (CO2-e) emissions: A comparison
- between geopolymer and OPC cement concrete, Constr. Build. Mater. 43 (2013) 125–
- 883 130. https://doi.org/10.1016/J.CONBUILDMAT.2013.01.023.
- 884 [39] P.K. MEHTA, P.J. MONTEIRO, Concrete: Microstructures, Properties, and Materials,
- 885 McGraw-Hill, 2014.
- 886 [40] Ruviaro, A. S., Santana, H. A., dos Santos Lima, G. T., Barraza, M. T., Silvestro, L.,
- Gleize, P. J. P., & Pelisser, F. Valorization of oat husk ash in metakaolin-based
- geopolymer pastes. **Construction and Building Materials**, v. 367, p. 130341, 2023.
- https://doi.org/10.1016/j.conbuildmat.2023.130341
- 890 [41] A. Obmiński, Asbestos cement products and their impact on soil contamination in
- relation to various sources of anthropogenic and natural asbestos pollution, Sci. Total
- 892 Environ. 848 (2022) 157275. https://doi.org/10.1016/J.SCITOTENV.2022.157275.
- 893 [42] S. Malinconico, F. Paglietti, S. Serranti, G. Bonifazi, I. Lonigro, Asbestos in soil and
- water: A review of analytical techniques and methods, J. Hazard. Mater. 436 (2022)
- 895 129083. https://doi.org/10.1016/J.JHAZMAT.2022.129083.
- 896 [43] M. Romagnoli, P. Sassatelli, M. Lassinantti Gualtieri, G. Tari, Rheological
- characterization of fly ash-based suspensions, Constr. Build. Mater. 65 (2014) 526–534.
- 898 https://doi.org/10.1016/J.CONBUILDMAT.2014.04.130.
- 899 [44] S. Dadsetan, H. Siad, M. Lachemi, M. Sahmaran, Extensive evaluation on the effect of
- glass powder on the rheology, strength, and microstructure of metakaolin-based
- geopolymer binders, Constr. Build. Mater. 268 (2021) 121168.
- 902 https://doi.org/10.1016/J.CONBUILDMAT.2020.121168.

- 903 [45] D.P. Bentz, A. Ardani, T. Barrett, S.Z. Jones, D. Lootens, M.A. Peltz, T. Sato, P.E.
- Stutzman, J. Tanesi, W.J. Weiss, Multi-scale investigation of the performance of
- 905 limestone in concrete, Constr. Build. Mater. 75 (2015) 1–10.
- 906 https://doi.org/10.1016/J.CONBUILDMAT.2014.10.042.
- 907 [46] C.K. Yip, J.S.J. Van Deventer, Microanalysis of calcium silicate hydrate gel formed
- 908 within a geopolymeric binder, J. Mater. Sci. 38 (2003) 3851–3860.
- 909 https://doi.org/10.1023/A:1025904905176/METRICS.
- 910 [47] C.K. Yip, J.L. Provis, G.C. Lukey, J.S.J. van Deventer, Carbonate mineral addition to
- metakaolin-based geopolymers, Cem. Concr. Compos. 30 (2008) 979–985.
- 912 https://doi.org/10.1016/J.CEMCONCOMP.2008.07.004.
- 913 [48] A. Antoni, A.A.T. Purwantoro, W.S.P.D. Suyanto, D. Hardjito, Fresh and Hardened
- Properties of High Calcium Fly Ash-Based Geopolymer Matrix with High Dosage of
- 915 Borax, Iran. J. Sci. Technol. Trans. Civ. Eng. 44 (2020) 535–543.
- 916 https://doi.org/10.1007/S40996-019-00330-7/FIGURES/9.
- 917 [49] A. Antoni, S.W. Wijaya, D. Hardjito. Factors Affecting the Setting Time of Fly Ash-
- 918 Based Geopolymer, Mater. Sci. Forum. 841 (2016) 90–97.
- 919 https://doi.org/10.4028/WWW.SCIENTIFIC.NET/MSF.841.90.
- 920 [50] F. Puertas, C. Varga, M.M. Alonso, Rheology of alkali-activated slag pastes. Effect of
- the nature and concentration of the activating solution, Cem. Concr. Compos. 53 (2014)
- 922 279–288. https://doi.org/10.1016/J.CEMCONCOMP.2014.07.012.
- 923 [51] K. Vance, A. Dakhane, G. Sant, N. Neithalath, Observations on the rheological response
- of alkali activated fly ash suspensions: the role of activator type and concentration,
- 925 Rheol. Acta. 53 (2014) 843–855. https://doi.org/10.1007/S00397-014-0793-
- 926 Z/FIGURES/12.
- 927 [52] A. Poulesquen, F. Frizon, D. Lambertin, Rheological behavior of alkali-activated
- metakaolin during geopolymerization, J. Non. Cryst. Solids. 357 (2011) 3565–3571.
- 929 https://doi.org/10.1016/J.JNONCRYSOL.2011.07.013.
- 930 [53] J.L. Provis, G.C. Lukey, J.S.J. Van Deventer, Do geopolymers actually contain
- 931 nanocrystalline zeolites? a reexamination of existing results, Chem. Mater. 17 (2005)
- 932 3075–3085. https://pubs.acs.org/doi/abs/10.1021/cm050230i (accessed September 27,
- 933 2022).
- 934 [54] Z. Sun, A. Vollpracht, Isothermal calorimetry and in-situ XRD study of the NaOH
- activated fly ash, metakaolin and slag, Cem. Concr. Res. 103 (2018) 110–122.
- 936 https://doi.org/10.1016/J.CEMCONRES.2017.10.004.

937	[55]	V.D. Glukhovsky, Ancient, modern and future concretes, in: Proceedings of the First
938		International Conference on Alkaline Cements and Concretes, Kiev, 1994: pp. 1–9.
939	[56]	R.D. Snee, G.F. Piepel, Assessing Component Effects in Formulation Systems,
940		Http://Dx.Doi.Org/10.1080/08982112.2012.731628. 25 (2012) 46-53.
941		https://doi.org/10.1080/08982112.2012.731628.
942	[57]	E. Najafi Kani, A. Allahverdi, J.L. Provis, Efflorescence control in geopolymer binders
943		based on natural pozzolan, Cem. Concr. Compos. 34 (2012) 25–33.
944		https://doi.org/10.1016/J.CEMCONCOMP.2011.07.007.
945		